Relationship between ground levelling measurements and radar satellite interferometric estimates of bog breathing in ombrotrophic northern bogs

Tauri Tampuu[1], Jaan Praks[2], Francesco De Zan[3], Marko Kohv [1], Ain Kull[1]

[1] Institute of Ecology and Earth Sciences, University of Tartu, Estonia
[2] School of Electrical Engineering, Aalto University, Finland
[3] Remote Sensing Technology Institute, German Aerospace Centre DLR, Germany

SUMMARY

Understanding the seasonal oscillation of peatland surface height initiated by changes in water table level (known as 'bog breathing') is key to improving spatial models of the water balance of bogs and their greenhouse gas exchanges with the atmosphere. Bog breathing has been studied locally via point-based measurements by telmatologists as well as over wider areas by the remote sensing community, in the latter case often without or with limited ground-truth validation. We aim to bring the two disciplines together by assessing the feasibility of validating Synthetic Aperture Radar (SAR) data from the Sentinel-1 satellite with in situ ground levelling data from nanotopes with different drainage status in two hemiboreal raised bogs. We demonstrate the continuous measurement of bog breathing using automatic ultrasonic levelling devices which shows that, during one growing season, bog breathing amounted to 11.6–14.7 cm in hollows, 6.9–7.5 cm in hummocks and 9.5–11.6 cm in haplotelmic nanotopes. Accounting for such relatively large vertical surface deformations remotely using the SAR Differential Interferometry (DInSAR) technique is prone to estimation errors owing to the so-called estimation ambiguity that occurs when deformation exceeds half the wavelength of the radar signal (2.77 cm for Sentinel-1). We approach the ambiguity problem by estimating deformation between consecutive SAR acquisitions (time separation 6 or 12 days) only. Remote and in situ measurements of bog breathing correlate moderately to very strongly (r_s = 0.82–0.93 in hummocks) even though, from time to time, all nanotopes except hummocks show surface deformations in just a single day that exceed the ambiguity threshold. This indicates that DInSAR surface deformation estimates contain useful information despite under-estimating larger changes, and DInSAR has high potential for the assessment of bog breathing. Our findings imply that DInSAR estimates in peatlands without ground validation should be interpreted with caution. To take full advantage of the plentiful data from Sentinel-1, the introduction of contextual information (e.g. temperature, precipitation and/or evapotranspiration data) could guide ambiguity resolution, as we demonstrate up to moderate correlation (r_s = 0.59 in a hollow) between precipitation and bog surface height.

KEY WORDS: bog drainage, InSAR, peatland, Sentinel-1, surface deformation

INTRODUCTION

Northern peatlands are significant pools of stored carbon (Leifeld & Menichetti 2018, Nichols & Peteet 2019), but peatlands can switch from being net sinks of greenhouse gases (GHG) to emitters (Blodau 2002) depending on the water regime, which is vulnerable to both climate change and direct human disturbance (Gorham 1991, Ojanen *et al*. 2010, Yu 2012, Webster *et al*. 2018). The porous sponge-like nature of peat, which allows it to adsorb and release water and trap gases, causes the peatland surface to fall and rise following the dynamics of the water table (WT) (Roulet 1991, Kellner & Halldin 2002, Dise 2009). GHG exchange is largely determined by peat moisture content, which is closely related to WT (Heikurainen *et al*. 1964); as well as by temperature, vegetation and nutrient status, all being in turn affected by WT. Therefore, understanding the seasonal oscillation of peatland surface height and volume, often referred to as 'bog breathing' (Roulet 1991, Kellner & Halldin 2002), is key to improving spatial models of greenhouse gas (GHG) exchange (CO_2, N_2O, CH_4) with the atmosphere (Fritz 2006, Dise 2009). Despite being a well-known phenomenon (Strack *et al*. 2006) and significant for climate change (Blodau 2002, Dise 2009, Howie & Hebda 2018), bog breathing has not been exhaustively studied and understood (Fritz 2006, Fritz *et al*. 2008, Morton & Heinemeyer 2019). Nor has the spatiotemporal variability of bog surface deformations been documented definitively (Fritz 2006, Bradley *et al*. 2022, Marshall *et al*. 2022). Assessment of bog breathing over vast and remote

peatland areas is feasible with the satellite Synthetic Aperture Radar (SAR) and differential interferometry technique (Differential InSAR or DInSAR) (Lees *et al.* 2018, Morton & Heinemeyer 2019). DInSAR has become a proven tool for globally quantifying surface displacements at millimetre level in many domains (Ferretti *et al*. 2001, Ferretti *et al*. 2007, Crosetto *et al.* 2016, Osmanoğlu *el al*. 2016, Biggs & Wright 2020). Thus, the availability of SAR data potentially opens a new era in the study of bog breathing by finally enabling the estimation of temporal (including seasonal) bog surface movements with sufficient spatial resolution over wide areas, in contrast to the few point measurements that were previously available from accessible study sites only.

SAR measures the amplitude and phase of the backscatter of the transmitted electromagnetic signal (Ferretti *et al*. 2007). In DInSAR, SAR phase images from the same orbital position (zero-baseline) at different times are combined (Bamler & Hartl 1998). When two phase images are combined in DInSAR, the resultant phase difference or phase change image known as interferogram indicates the change in the targets during the time interval between two SAR acquisitions (Ferretti *et al*. 2007). Assuming that the dielectric properties of a target remain stable, the interferometric phase (DInSAR phase, i.e. phase change) becomes a sensitive measure of the surface elevation change (vertical deformation) (Bamler & Hartl 1998, Ferretti *et al*. 2007). In DInSAR, an elevation change smaller than half of the radar wavelength can be translated to a phase change inside a 360 degree or 2π radian circle, called the phase cycle, and can be measured precisely. Unfortunately, if the elevation change is larger than half of the wavelength, the phase jumps from 2π radian to 0 and repeats the cycle. This happens after every half-wavelength and, thus, possibly many times. Such periodicity brings 2π ambiguity to the relationship between the elevation change and the phase change. Therefore, in an interferogram, the real surface deformation is ambiguously wrapped in 2π phase cycles. The amount of height change that leads to a 2π change in the sensor's line of sight (LOS) phase change (Rosen *et al*. 2000) is referred as the LOS ambiguity threshold in this paper. Whenever the surface deformation is larger than the LOS ambiguity threshold, phase unwrapping, i.e. addition of the correct number of phase cycles to the phase change, is needed to resolve the phase ambiguity and reconstruct the true elevation change (Ferretti *et al*. 2007). The unwrapping issue is central to obtaining accurate deformation estimates. The key to the correct ambiguity resolution is a visible fringe pattern in the interferogram. A fringe occurs when the phase jumps from +1π radian to −1π radian or vice versa, often referred to as a phase jump. Assuming that the true phase gradient is continuous because the surface of a natural terrain is elastic, a phase jump visible in the interferogram is not caused by an abrupt shift of a part of the observed surface (Bamler & Hartl 1998, Ferretti *et al*. 2007). For further explanation of the theory of DInSAR in the context of studying northern bogs, refer to Tampuu (2022).

Despite having revolutionised measurement of the Earth's surface deformation globally (Biggs & Wright 2020), DInSAR has seen limited application over peat. This is because the majority of DInSAR methods are suitable primarily for non-vegetated surfaces where DInSAR coherence, which describes local phase stability (Ferretti *et al*. 2007), is high (Alshammari *et al*. 2018). Therefore, DInSAR studies in northern peatlands have been concerned mainly with long-term peatland subsidence using advanced DInSAR techniques, referred to collectively as InSAR time series analysis, which can mitigate the coherence issue (Zhou 2013, Cigna & Sowter 2017, Alshammari *et al*. 2018, Fiaschi *et al*. 2019).

A limited number of publications have only recently dealt with bog breathing. To the best of our knowledge, the inclusive list contains Alshammari *et al*. (2020), Tampuu *et al*. (2020), Tampuu *et al*. (2021a), Bradley *et al*. (2022), Marshall *et al*. (2022) and Tampuu *et al*. (2022). Among these, only Marshall *et al*. (2022), Tampuu *et al*. (2021a) and Tampuu *et al*. (2022) possessed ground levelling measurements to compare with the surface oscillation derived using DInSAR. The last two describe our own preliminary research, and use the same ground validation data as this study but larger windows in coherence estimation and phase filtering. In the current article we have reduced the estimation windows as a trade-off between minimising averaging-out of the useful signal and increased noise.

The absence of ground levelling data for validation has been characteristic for the entire field of peatland DInSAR (Cigna & Sowter 2017, Alshammari *et al*. 2018). Another issue, outwith the scope of this study, is the representativeness of point measurements for spatially much larger footprints, such as a SAR pixel, in bogs with high nanotope-level heterogeneity (Alekseychik *et al*. 2021, Marshall *et al*. 2022).

The estimates of bog breathing sensed with DInSAR by Alshammari *et al*. (2020), Tampuu *et al*. (2020) and Bradley *et al*. (2022) and not validated with in situ levelling were internally consistent and related to peatland ecohydrology, but were considerably smaller in magnitude than the known possible amplitude of bog breathing (Glaser *et al.*

2004, Fritz 2006, Howie & Hebda 2018). Alhough Zhou (2013), Alshammari *et al*. (2018) and Tampuu *et al*. (2020) anticipated the risk of unwrapping errors in bogs, research has only recently provided some evidence, based on ground data, for the unreliability of C-band (Conventional band; wavelength ~5.6 cm) DInSAR time series analysis in peatlands. Marshall *et al*. (2022) demonstrated under-estimation during a drought period and in more dynamic areas of blanket bog, while Heuff & Hanssen (2020) and Conroy *et al*. (2022) showed that erroneously resolved phase ambiguities made estimates for grasslands on peat unreliable, and Umarhadi *et al*. (2021) showed the peat subsidence rate based on C-band time series was underestimated compared to results based on L-band (Long band; ~24 cm) and on surface deformations modelled from the WT in tropical peatlands.

Phase unwrapping in natural landscapes can be very complicated and, when incorrectly solved, leads to wrong deformation estimates (Alshammari *et al*. 2018). To avoid the ambiguity issue, Marshall *et al.* (2022) recommended using interferometry in less dynamic parts of the peatland. To tackle the ambiguity issue, Conroy *et al*. (2022) proposed the introduction of contextual information, i.e. temperature and precipitation, to guide unwrapping.

The estimation of elevation changes smaller than the LOS ambiguity threshold is intrinsically least error-prone (Conroy *et al*. 2022). Reducing the temporal baseline (i.e. time interval) between the image pairs constituting an interferogram is the simplest way to reduce the magnitude of change (Alshammari *et al*. 2018, Conroy *et al*. 2022). Tampuu *et al*. (2020) and Tampuu *et al*. (2021b) have shown that coherence is preserved in open raised bogs over short to medium time intervals (i.e. days to months), indicating that applying conventional short temporal baseline DInSAR (using only radar acquisitions whose time separation is short, i.e. days) is possible in open bogs and can produce reliable deformation results. Until now, ground measurements have only been compared with deformation estimates from InSAR time series analysis (Alshammari *et al*. 2018, Marshall *et al*. 2022). The conventional DInSAR approach has been largely ignored and, to the best of our knowledge, used only by Tampuu *et al*. (2021a) and Tampuu *et al*. (2022). However, limiting the analysis to only the shortest baselines may capture surface movements that are beyond the scope of advanced DInSAR.

Bog breathing has been studied locally via point-based measurements by telmatologists, as well as over wider areas by the remote sensing community, in the latter case often without or with limited ground-truth validation. We aim to bring the two disciplines together by assessing the feasibility of using Sentinel-1 C-band SAR data validated with time series of in situ ground levelling data from raised bog nanotopes with different drainage status. The objectives of this study are:

1. to assess the accuracy of Sentinel-1 conventional short temporal baseline DInSAR in estimating bog breathing by comparing the results with automatically measured continuous in situ ground levelling measurements from different nanotopes in two raised bogs in Estonia over the growing season of 2016;
2. to discuss implications for the applicability of DInSAR to monitoring bog breathing; and
3. to publish the in-situ ground levelling data from different nanotopes along a gradient of decreasing drainage influence.

Continuous records of in situ bog breathing are rare in any case, and particularly rare if they address the gradient of drainage influence. Only the shortest available time intervals (6 or 12 days) are used for estimating DInSAR surface deformation, to minimise the need for phase unwrapping, and we hypothesise that this can allow accurate assessment of the magnitude of bog breathing because the magnitude of surface deformations will be small enough to remain within the convenient range for C-band radar.

MATERIALS

Study area

This study is concerned with two medium-sized ombrotrophic mires (bogs) in Estonia (Figure 1). Umbusi Bog (58.57 °N, 26.18 °E) and Laukasoo Bog (58.43 °N, 27.00 °E), located 50 km apart, are characteristic of hemiboreal (northern temperate) raised bogs. Both bogs have a deep peat layer and a pool system in the central part of the bog. The peat thickness at our study transects is ~ 8 m in Umbusi and ~ 5 m in Laukasoo. At each site, the *Sphagnum*-dominated open bog is a ridge-hollow-hummock ecotope while the central part is a ridge-pool ecotope dominated by *Pinus sylvestris* trees up to 5 m tall. The growing season in Estonia usually lasts from early May to the end of October. Precipitation (annual norm 672 mm) is unevenly distributed with a minimum in winter–spring and a maximum in summer–autumn. The bog water table (WT) is highest during snowmelt in April, lowers rapidly in May and June due to high subsurface discharge and evapotranspiration, and usually reaches a minimum level in July or August. In autumn, the peat pore water recharges due to decreasing evapotranspiration

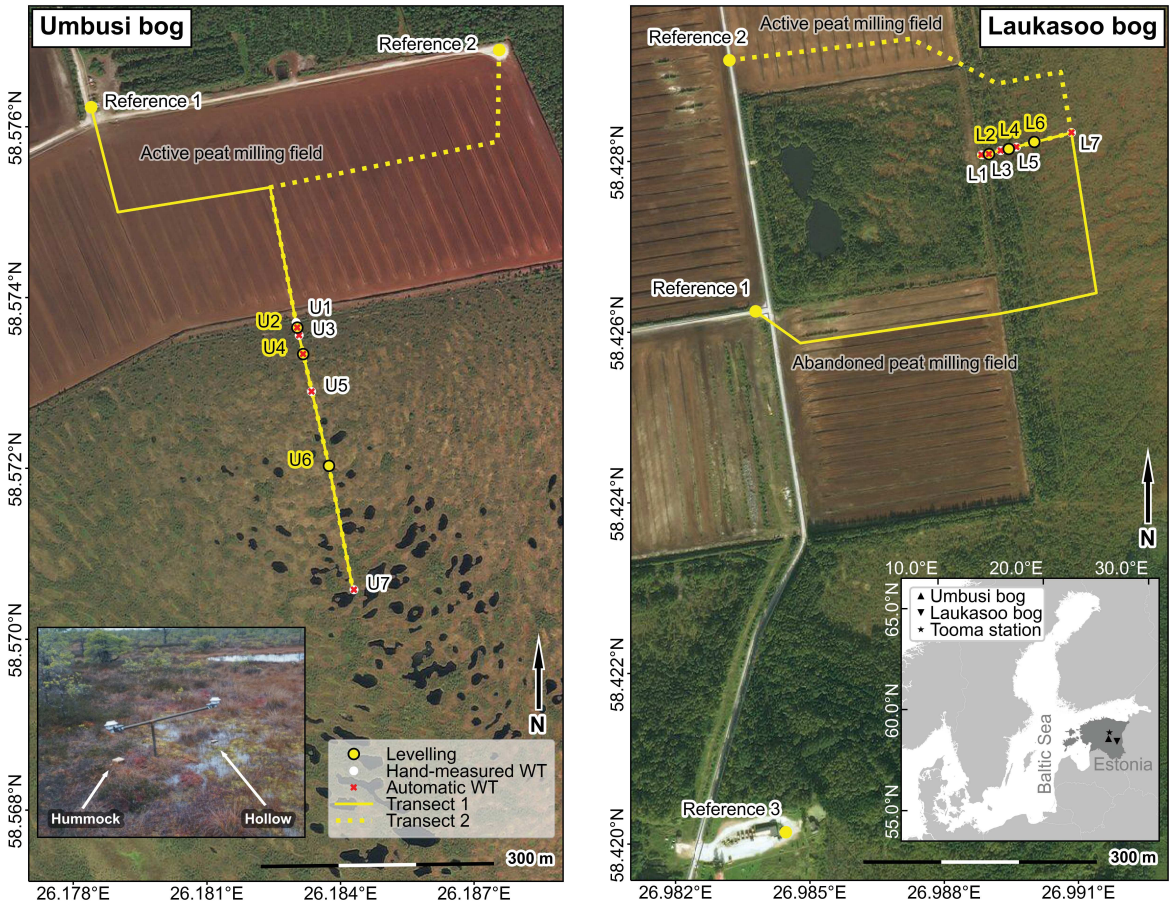

Figure 1. Plan views of the transects on Umbusi Bog (left) and Laukasoo Bog (right) in relation to the milled peat extraction areas. At each site a transect of plots with automatically and manually measured bog water table (WT) and automatic surface levelling measurements follows the gradient of decreasing drainage influence from the drainage ditch to the interior of the open natural bog. Each transect is prolonged towards the reference plots as two virtual transects crossing peat extraction fields. The letters "U" for Umbusi and "L" for Laukasoo, together with the plot identifiers, denote measurement plots. The levelling device recording both a hollow and a hummock nanotope at Plot U6 is shown in the inset image for Umbusi Bog. The location of Tooma Meteorological Station is shown in the inset map.

and increased precipitation, and a rise of the WT follows. The bog surface freezes and snow cover establishes in December, and the snow persists until April (Estonian Environment Agency 2023).

In both bogs, the natural bog area is truncated by an active milled peat extraction area with a system of double-ditch drainage. The border between the peat extraction field and natural bog is formed by the main drainage ditch which cuts through the entire peat layer. Running parallel to that main drain, at 15–20 m in the direction of the centre of the bog, there is a secondary drainage ditch (~0.5 m deep) which penetrates the acrotelm. The margins of the bog sections that are affected by drainage are wooded (*Pinus sylvestris*).

Measurement transects along the gradient of drainage influence

A transect of automatic surface levelling and WT measurements has been established along the gradient of decreasing drainage influence in both Umbusi Bog and Laukasoo Bog (Figure 1). Both transects, consisting of seven measurement plots (plots 1–7), stretch from the main drainage ditch into the intact portion of the natural bog. The transects were initially established to measure bog WT manually in WT sampling wells, at monthly intervals. Automatic WT measurement and surface levelling devices were installed later, at some of the plots. The naming convention employed for the measurement plots follows a spatial logic: uppercase

letter denotes the bog (U for Umbusi Bog, L for Laukasoo Bog); the plot identifier (integer) denotes the position of the plot in relation to the gradient of decreasing drainage influence (plots numbered 1–7, with 1 closest to and 7 farthest from the drainage ditch). The levelling measurements at Plots U6 and L6 are recorded in both a hollow and a hummock nanotope, with the distance between the measuring devices being 2 m and distinguished by the respective subscripts "hol" and "hum". The transects used in this study are part of a wider study focusing on the effects of drainage on bogs and transitional mires. Detailed descriptions of the layout of transects and other studied factors are provided by Paal *et al*. (2016).

In this article we are concerned only with the six measurement plots (U2, U4, U6 in Umbusi Bog and L2, L4, L6 in Laukasoo Bog) for which surface levelling data are available over the 2016 growing season (15 Apr to 31 Oct). Automatic WT data from the selected (levelling) plots are also considered if available. If automatic WT data are not available from the same plot, the manually measured WT data are used to decide whether automatic WT measurements from a neighbouring plot can be used to represent the WT at the levelling plot.

The haplotelmic plots U2 and L2 (characterised by no acrotelm and compacted peat) are located around 15 m from the main drain and are severely affected by drainage. Plots U4 (lawn nanotope) and L4 (hollow nanotope) experience a significant influence of drainage, being located ~ 50 m and ~ 40 m from the main drain in Umbusi Bog and Laukasoo Bog, respectively. Plots U6 and L6 are located in ridge-hollow-hummock microtopes within zones which are intact in terms of most factors but experience a weak influence of drainage according to some of our metrics. This assessment is based on 107 indicators (characteristics of vegetation, nutrients, water regime, water chemistry, nanotope structure, landscape metrics, etc.). All of the indicators are given in a report in Estonian (Kull 2016) and some of them (for transitional mires) have been published in English (Paal *et al.* 2016). As a simplification in this study we consider Plots U6 and L6 to be natural sites, lying 200 m and 75 m from the main drains in Umbusi Bog and Laukasoo Bog, respectively.

Automatic and manual water table measurements

The automatic WT measurements were obtained using automatic piezometers (Geotech AB, Göteborg, Sweden) and values are recorded as daily averages for 2012–2018. In the case of Umbusi Bog, automatic WT measurements are available from Plots U2, U4, U5 and U7 except that data for the period 26 May–25 June 2016 are missing. With regard to Laukasoo Bog, the automatic WT data are from Plots L1, L2, L3 and L7. The piezometers were installed in the stable peat layer at 1.3 m depth (from the surface at the time of installation) and measure the pressure of the water column. The barometrically compensated WT level relative to the peatland surface was modelled from the water and air pressures. The WT data calculated from piezometer readings were validated using manual WT measurements in sampling wells located near the piezometers. The sampling wells were anchored in the stable peat layer 1.3 m below the mire surface at the time of installation. WT in the sampling wells was recorded relative to the peatland surface at monthly (or bi-monthly) intervals year-round in 2012–2016.

Automatic surface levelling measurements

From the plots numbered 2, 4 and 6 in both bogs (U2, U4, U6 in Umbusi Bog and L2, L4, L6 in Laukasoo Bog), we have time series of automatic ground levelling measurements over the growing season of 2016. For this we built devices that measure the time an ultrasound wave takes to travel along the path sensor–ground–sensor and convert this time into the distance between the sensor and the ground (resolution 0.25 mm, repeatability ± 0.2 % / ± 1 mm). Each device was attached to a T-shaped metal bar that penetrated through the peat layer and was anchored in the underlying stable mineral ground. At Plots U6 and L6, one device recorded the surface elevation in a hollow ($U6_{hol}$ and $L6_{hol}$) and another was placed in a hummock ($U6_{hum}$ and $L6_{hum}$), with the distance between the two devices being 2 m. At Plots U2, L2, U4 and L4, only one device was used. Since only daily average data were available for L2, all of the hourly levelling data were aggregated to daily data. The time series end when the levelling devices were removed after the formation of snow cover, which prevents the signal from reaching the ground. Additionally, fog and intense rain may occasionally cause inaccuracies in the measurements.

Meteorological data

Precipitation data (2012–2018) were provided by the Estonian Environment Agency as daily totals from Tooma Meteorological Station (Estonian Environment Agency 2021), which is located 35 km north of Umbusi Bog and 65 km northwest of Laukasoo Bog (Figure 1 inset) and considered to be representative of both locations. The growing season (15 Apr to 31 Oct) of 2016, which is in the focus of this study, was climatologically close to normal except that May and September were drier than normal with 16 mm vs. 42 mm and 28 mm vs. 64 mm of rainfall, respectively.

SAR data

The SAR data were collected by the radar satellite mission Sentinel-1 (S1), consisting of a constellation of two identical satellites, S1A and S1B. The images we used cover the period 01 Jul to 29 Oct 2016, which is limited by the availability of S1 summer acquisitions between periods when S1 operated in Extended Wide (EW) swath mode for sea-ice monitoring and ground levelling data in autumn. We used 14 S1A and S1B ascending orbit (relative orbit number 160) vertical-vertical (VV) polarisation Interferometric Wide (IW) swath mode Single Look Complex (SLC) images. As S1B started operation in April 2016 and the first image over our study areas is dated 29 Sep 2016, we could use three S1B acquisitions in our stack. The acquisition time is around 15.56 UTC, corresponding roughly to 19.00 EEST, the local time of our study area. The local incidence angle in the sub-swath IW2 is 38.41° over Umbusi Bog and 40.96° over Laukasoo Bog. The pixel spacing in IW2 approximates to 4 m × 14 m (range (rg) × azimuth (az)) on the ground and the spatial resolution is 3.1 m × 22.7 m (rg × az) (CLS 2016). Thus, the S1 data are much coarser than a single nanotope on the bog and the backscattering response is formed at the level of the microtope, which consists of a pattern of nanotopes (Lindsay 2010). The interferometric baselines (the distance between the image acquisitions) vary roughly from -5 to 140 metres.

METHODS

Correlating in situ measurements of bog breathing and DInSAR deformation estimates

The aim of the DInSAR analysis was to correlate the measured seasonal vertical surface deformation on the open natural bog with Sentinel-1 DInSAR deformation estimates. The deformation estimates were calculated using the conventional short temporal baseline (6 or 12 days) DInSAR method to take into account possible large magnitudes of bog breathing. The DInSAR deformation estimates were compared to ground levelling measurements from different nanotopes along the drainage gradient in the raised bog.

In Umbusi Bog, 13 interferograms for Plot U4 and 11 interferograms for Plots $U6_{hol}$ and $U6_{hum}$ were used in the analysis. In Laukasoo Bog, 11 interferograms for Plots L4 and $L6_{hum}$ and 13 interferograms for plot $L6_{hol}$ were used. Plots U2 and L2 were excluded from the DInSAR analysis because they were located a mere 15 m from the drain and were thus potentially susceptible to pixel contamination by the drainage ditch and the peat extraction field. Also, significant tree cover and shrubs resulting from the direct effects of drainage could potentially cause decorrelation of the DInSAR phase. Conventionally, coherence (γ) thresholds have been set to extract more reliable pixels (Berardino *et al*. 2002, Jiang & Lohman 2021). However, despite its common use there is no prescribed value for such a threshold, as the coherence bias depends upon the resolution (sensor-dependent) and the applied coherence estimation window size (Morishita & Hanssen 2015). Here we use a threshold of $\gamma = 0.4$ to ensure more reliable phase estimates in concordance with previous research (Weydahl 2001, Mohammadimanesh *et al*. 2018, Braun & Veci 2020).

DInSAR processing

The interferograms, which contain unprocessed interferometric phase and coherence estimates, were computed using SARPROZ software (Perissin 2021). For the interferometric coherence estimation (weighted by the amplitude; calculated before filtering) and Modified Goldstein phase filtering (Goldstein & Werner 1998), a window of ten pixels in range and three in azimuth direction was used, approximating to a 40 m square footprint on the ground. The 40 m length for the footprint was chosen to best address the trade-off between the coherence estimation bias towards higher values and the loss of spatial resolution (Touzi *et al*. 1999). Flattening and topographic phase removal were applied. No multi-looking was applied in order to preserve the original pixel's spatial resolution, as natural bog displays high nanotope and microtope level heterogeneity with hummocks, ridges and hollows occurring at a spatial scale of 0.5–10 m.

Formation of DInSAR deformation transects for further analysis

For the interferograms, only the pixels corresponding to the measurement transects were selected for analysis, and the pixels located over the ground levelling measurement plots were correlated with the ground levelling measurements. To calibrate the DInSAR phase measurements, a known stable reference point is needed. In the absence of ground calibration data, locations from the stable mineral soil or compacted haplotelmic organic soil were used as stable reference points where zero displacement in any direction (vertical or horizontal) is assumed (following the example by Liu *et al*. 2010). To study the influence of the coherence of the chosen reference point on the final result, we used multiple reference points for both bogs. In Umbusi Bog the independent reference points used were a cluster of small

buildings and an extension to the causeway, while in Laukasoo Bog a larger building, a junction and a causeway were used (Figure 1).

This simplified approach of assuming zero displacement at a stable reference point in all the images allowed us to also neglect the atmosphere induced errors in the phase, as the atmosphere should stay relatively constant over a few kilometres (Webley *et al*. 2004, Foster *et al*. 2006, Bekaert *et al*. 2015). The maximum distance from any point in the transect to the stable reference point was 560 m in Umbusi and 960 m in Laukasoo. The DInSAR line of sight (LOS) deformation (i.e. altitude change) measurements were projected into the vertical direction (u_{LOS}) using local incidence angles, assuming no horizontal motion in the peat (following the work by Hoyt *et al*. 2020). Regarding minimal temporal baselines and corresponding negligible crustal motions (Lidberg *et al*. 2010), we were not concerned with horizontal ground motion (Fuhrmann & Garthwaite 2019). All calculations were carried out in the SAR coordinates.

We extended each ground levelling transect virtually over the peat extraction fields to create continuous phase value paths (assuming a deformation gradient along the elevation change profile) from two reference points to the measurement points (Figure 1). The phase difference between the points along a transect was treated as a difference in the deformation between imaging dates, assuming the reference point was stable. To avoid phase ambiguity, the whole phase dynamics between a reference point and measurement points were fitted into a single phase cycle (2π radians, which corresponds to half of the wavelength of the sensor, being ~2.77 cm for Sentinel-1). This was done by adding a constant to the complex phase value, which does not affect the calculated phase difference. In this way, the linear relationship between the assumed deformation gradient and the phase could be maintained and assured with a visual interpretation of the DInSAR deformation profile along the virtual transect without the need for phase unwrapping as long as the profile did not indicate a phase jump. If the transect-and-phase-rotation based approach had not been implemented, the phase at the reference point would have been set to zero and, consequently, the unambiguous change would have been confined to being found in $\pm 1\pi$ (a quarter of the radar wavelength) (Novellino *et al*. 2017, Esch *et al*. 2019).

The Umbusi virtual transects 1 and 2 and Laukasoo transect 2 crossed active peat extraction fields whereas Laukasoo transect 1 extended over an abandoned peat milling field. Laukasoo reference point 3 was not connected to the measurement points via a transect because there was intervening forest which caused decorrelation in the radar signal. For Laukasoo reference point 3 the phase rotation from the nearest transect, i.e. Laukasoo transect 1, was used.

Data analysis

All the data were analysed in Python programming language version 3.6 (Python Software Foundation 2021). The hourly ground levelling data were cleaned of outliers using the Tukey's fence method with a multiplier of 1.5 (Tukey 1977) in a discrete 3-day window, and presented as daily median (except for Plot L2 where only daily averages were available). As the data were not normally distributed according to the Shapiro-Wilk test for normality (Shapiro & Wilk 1965), the Spearman's rank-order correlation (Spearman 1904) was applied to estimate the correlation between the levelling, DInSAR and WT data. Reporting of the strength of correlation follows the convention: negligible (0.0–0.3), weak (0.3–0.5), moderate (0.5–0.7), strong (0.7–0.9), very strong (0.9–1.0). The threshold of statistical significance is p-value < 0.05.

To enable comparison of the calculated DInSAR u_{LOS} deformation estimates between two consecutive SAR acquisitions with the in situ surface levelling measurements, we calculated the ground-measured vertical deformation of the peatland surface between the dates corresponding to each interferometric pair. The time separation was either 6 or 12 days depending on the interferometric pair. Additionally, to better understand how large and rapid the short-term peatland surface deformations caused by bog breathing can be, we calculated the vertical surface deformation for every possible 1-day and 6-day period from the levelling measurements. The overlapping measurement period for all of the levelling devices was 25 Apr to 07 Oct 2016.

RESULTS

Bog breathing

The range of bog breathing at our study plots during the growing season (15 Apr to 31 Oct) of 2016 is shown in Table 1, where the surface elevation is given relative to the maximum surface height during the measurement period. The largest surface deformations were recorded in natural hollow nanotopes, at Plot $L6_{hol}$ on Laukasoo Bog (median surface level -4.3 cm, minimum level -14.7 cm) and at Plot $U6_{hol}$ on Umbusi Bog (median -5.7 cm, minimum -12.6 cm). The haplotelmic plots U2 and L2 also displayed large surface fluctuations (median surface level -5.4 cm, minimum -9.5 cm at U2;

Table 1. The magnitude of bog breathing and water table (WT) changes in Umbusi Bog and Laukasoo Bog during the growing season (15 Apr–31 Oct) of 2016 and the growing seasons in 2012–2018. The daily median for the period is given with the range of changes in parentheses. Bog breathing is given relative to the maximum surface height recorded during the period, and WT is shown relative to the peatland surface. The letters "U" and "L" (together with the plot identifier) denote measurement plots along the drainage gradient in Umbusi Bog and Laukasoo Bog, and levelling measurements for hollow and hummock nanotopes at Plots U6 and L6 are denoted by the subscripts "hol" and "hum", respectively. The WT values from Plots U5, L3 and L7 are applied, respectively, to Plots U6, L4 and L6, where WT was not measured.

Plot	Bog breathing 2016 median (range) in cm	WT 2016 median (range) in cm	WT 2012–2018 median (range) in cm
U2	-5.4 (-9.5 to 0.0)	-53.1 (-68.3 to -38.6)	-74.6 (-114.2 to -38.6)
U4	-5.7 (-10.8 to 0.0)	-26.9 (-41.7 to -13.4)	-35.4 (-63.0 to -6.0)
U5		-29.0 (-36.9 to -22.4)	-33.5 (-57.7 to -13.7)
$U6_{hol}$	-5.7 (-12.6 to 0.0)	U5	U5
$U6_{hum}$	-3.3 (-7.5 to 0.0)	U5	U5
L2	-3.9 (-8.0 to 0.0)	-29.2 (-45.6 to -22.8)	-40.3 (-84.3 to -12.7)
L3		-21.8 (-27.5 to -16.0)	-24.9 (-48.6 to -9.0)
L4	-3.3 (-11.6 to 0.0)	L3	L3
$L6_{hol}$	-4.3 (-14.7 to 0.0)	L7	L7
$L6_{hum}$	-2.2 (-6.9 to 0.0)	L7	L7
L7		-14.2 (-18.2 to -6.7)	-16.1 (-39.5 to 2.0)

median -3.9 cm, minimum -8.0 cm at L2). The smallest surface fluctuations were recorded in natural hummock nanotopes, at $L6_{hum}$ (median -2.2 cm, minimum -6.9 cm) and $U6_{hum}$ (median -3.3 cm, minimum -7.5 cm). In other words, bog breathing larger in range than the Sentinel-1 sensor's LOS ambiguity threshold (~2.77 cm) was recorded in all observed nanotopes of both bogs indifferently of the nanotope's disturbance status.

The largest short-term deformations were recorded at Plot L4 in Laukasoo. Here the change in surface level during a single day exceeded ~2.77 cm on 28 occasions (Table 2), with subsidence occurring on 13 of these occasions (range -3.2 to -7.8 cm, median -5.0 cm) and surface rise occurring on 15 occasions (range 3.0 to 6.6 cm, median 4.1 cm); and during 6-day periods there were 58 instances of changes larger than the ambiguity threshold. Only the natural hummock plots $U6_{hum}$ and $L6_{hum}$ exhibited surface fluctuations that were consistently less than the Sentinel-1 sensor's LOS ambiguity threshold of ~2.77 cm.

Water table fluctuations

The WT (relative to the peatland surface at the time of measurement) recorded by the automatic piezometers was highest and changed least at Plot L7 (Table 1). At the natural bog plot L7, the median WT during the 2016 growing season was -14.2 cm, range -18.2 to -6.7 cm. The long-term (2012–2018) median growing season WT at Plot L7 was -16.1 cm, range -39.5 to 2.0 cm. The WT was lowest and fluctuated over the greatest range at the haplotelmic plot U2 (median level -53.1, range -68.3 to -38.6 in 2016; median level -74.6, range -114.2 to -38.6 in 2012–2018).

Correlation between water table and bog breathing

To study the connection between WT and bog surface height we correlated the automatic piezometer readings with the levelling measurements. As we had levelling measurements but no automatic WT measurements from Plots U6, L4 and L6, we used the manual (2012–2016) WT readings from the sampling wells (average values shown in Table 3) to judge

Table 2. Occasions when bog breathing exceeded the Sentinel-1 sensor's line of sight ambiguity threshold (~2.77 cm) in Umbusi Bog and Laukasoo Bog in any given 1-day and 6-day period during 2016 (the overlapping measurement period for the levelling devices was 25 Apr to 07 Oct). The total count (N) of such occasions is given, with subsidence (-) distinguished from rise (+). The data presented are medians of bog surface change with the range in parentheses. The letters "U" and "L" (together with the plot identifier) denote measurement plots along the drainage gradient in Umbusi Bog and Laukasoo Bog, and levelling measurements from the hollow and hummock nanotopes at Plots U6 and L6 are denoted by the subscripts "hol" and "hum", respectively.

Plot	Nanotope	1-day period					6-day period				
		N	N-	Subsidence (cm)	N+	Rise (cm)	N	N-	Subsidence (cm)	N+	Rise (cm)
U2	haplotelmic	1	1	-2.9			7	1	-3.0	6	3.3 (3.0 to 5.0)
L2	haplotelmic	6	3	-4.1 (-4.8 to -3.0)	3	4.3 (2.9 to 5.1)	10	2	(-3.9 to -3.7)	8	3.2 (3.1 to 4.7)
U4	lawn	0					4			4	3.3 (3.0 to 3.6)
L4	hollow	28	13	-5.0 (-7.8 to -3.2)	15	4.1 (3.0 to 6.6)	58	30	-4.7 (-8.6 to -3.0)	28	4.3 (3.0 to 8.4)
$U6_{hol}$	hollow	0					7			7	3.5 (3.0 to 4.1)
$L6_{hol}$	hollow	4	1	-3.0	3	3.2 (3.0 to 3.5)	19	1	-3.2	18	3.6 (3.0 to 5.9)
$L6_{hum}$	hummock	0					0				
$L6_{hum}$	hummock	0					0				

Table 3. Weighted averages of monthly (2012–2016) manual water table (WT) measurements in the sampling wells at Umbusi Bog and Laukasoo Bog. WT is recorded relative to the peatland surface. Distance from the main drainage ditch is shown. The letters "U" and "L" (together with the plot identifier) denote measurement plots along the drainage gradient in Umbusi Bog and Laukasoo Bog, respectively.

	Plot	U1	U2	U3	U4	U5	U6	U7
Umbusi Bog	Distance (m)	10	16	26	51	101	201	365
	Average WT (cm)	-77.2	-64.2	-42.9	-26.8	-11.8	-12.2	-2.9
	Plot	L1	L2	L3	L4	L5	L6	L7
Laukasoo Bog	Distance (m)	3	13	28	38	50	75	125
	Average WT (cm)	-114.9	-26.5	-7.0	-16.6	-5.6	-0.4	-7.5

which of the piezometers could best represent the WT at each of these three plots. Guided by this exercise, we applied the piezometer data from Plot U5 to Plot U6, that from L3 to L4, and that from L7 to L6 in further analysis (Table 1).

Figure 2 shows the dynamics of surface height in adjacent (2 m apart) natural hollow and hummock nanotopes in relation to WT measured by the corresponding piezometers in Umbusi Bog (Plots $U6_{hol}$, $U6_{hum}$ and U5) and Laukasoo Bog (Plots $L6_{hol}$, $L6_{hum}$ and L7). The dynamics for haplotelmic and drainage affected plots are shown in Figure A1 in the Appendix. In general, the relationship between WT and bog breathing can be expected to differ between natural areas with intact acrotelm and haplotelmic parts of the bog. In bog with an acrotelm, the bulk density of the surface layer is low, leading to smooth surface movements that correlate directly with WT changes. In haplotelmic parts, bulk density is higher, rewetting takes longer and fast reactions to WT changes are rare, but seasonal surface height changes can be of similar magnitude to those in natural bog.

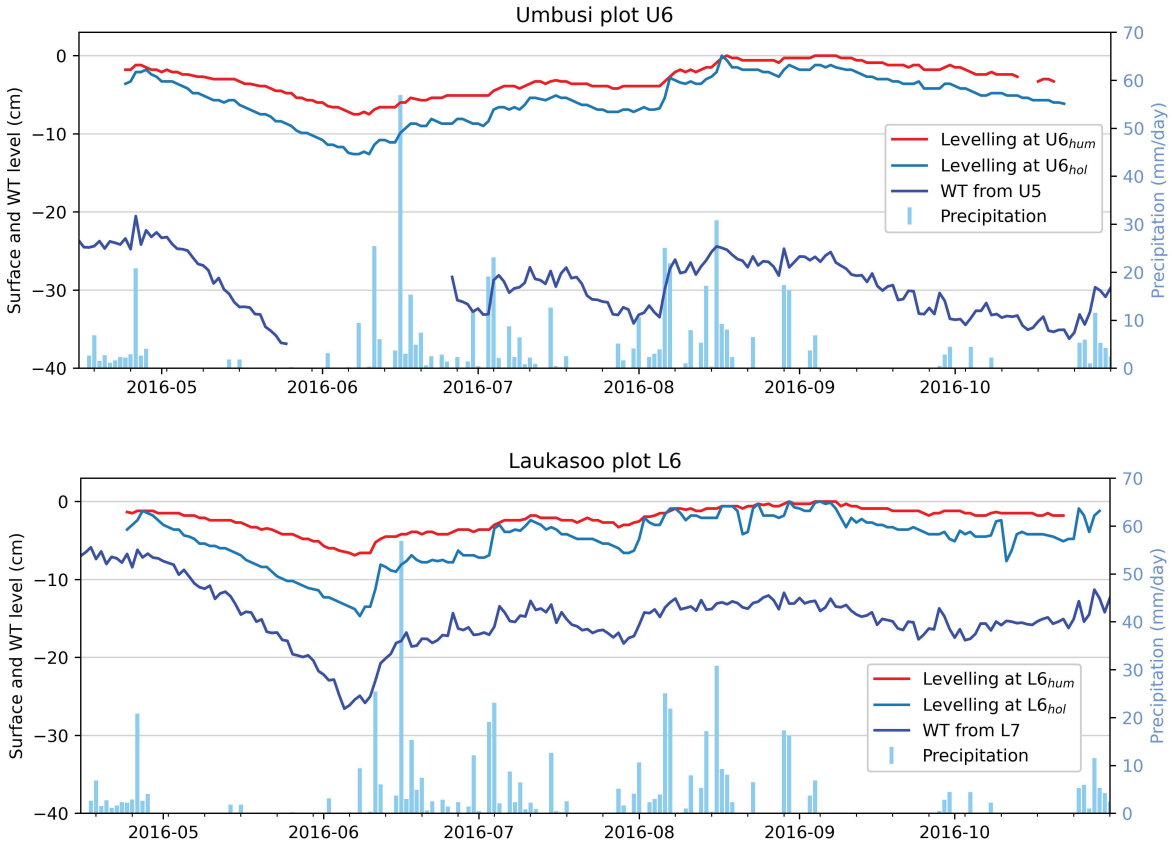

Figure 2. The daily median of peatland surface height and the daily average of water table depth (WT) for Plot U6 in Umbusi Bog and Plot L6 in Laukasoo Bog where levelling data are available, along with daily precipitation during the growing season (15 Apr–31 Oct) in 2016. The levelling data are relative to the maximum surface height during the period. Levelling measurements from hollow and hummock nanotopes are denoted by the subscripts "hol" and "hum", respectively. The WT data are relative to the peatland surface at the time of measurement. The WT measurements from Plot U5 are used to represent WT at U6 in Umbusi and the WT measurements from Plot L7 are used to represent WT at L6 in Laukasoo.

The correlation between surface height and WT (Table 4) in Umbusi Bog was strong at Plots U4 and $U6_{hol}$ and moderate at Plots $U6_{hum}$ and U2. The correlations were weaker overall in Laukasoo Bog, being strong at Plot L2 (haplotelmic), moderate at Plots $L6_{hol}$ and $L6_{hum}$, and weak at Plot L4. All correlations were statistically significant at both sites. The intra-seasonal dynamics of WT and surface height are detailed in Figure A2.

Correlation between precipitation, water table and bog breathing

The correlation between the surface height, WT and cumulative precipitation of the preceding time periods during the growing season in 2016 is shown in Table 4. Both surface height and WT correlated most strongly to the cumulative precipitation of the preceding 12 days. The correlation with 12-day precipitation was statistically significant at all measurement plots. In Laukasoo the correlation between surface level and 12-day precipitation was moderate at Plot $L6_{hol}$ and weak at Plot $L6_{hum}$, whereas in Umbusi this correlation was weak at $U6_{hol}$ and negligible at $L6_{hum}$. The correlation between WT and 12-day precipitation was moderate at Plot U4 in Umbusi Bog and at Plots L2 and L3 in Laukasoo Bog. The correlations of WT with precipitation sums for less than nine preceding days were variable, ranging from negligible to moderate. In general, precipitation showed stronger explanatory power over WT than over surface height. Also, the explanatory power was stronger for hollows than for hummocks (Table 4). Over the long term (growing seasons 2012–2018), the correlation of WT with the precipitation sum of

Table 4. Correlations between the daily median of automatically measured bog surface level, water table (WT) in the corresponding wells and the cumulative daily precipitation sum (Pr.) of the preceding 1, 6, 9, 12, 15 and 18 days during the growing season (15 Apr–31 Oct) of 2016. WT is relative to the peatland surface. 118 days have been correlated. The letters "U" and "L" (together with the plot identifier) denote measurement plots along the drainage gradient in Umbusi Bog and Laukasoo Bog, and levelling data from hollow and hummock nanotopes at Plots U6 and L6 are distinguished by the subscripts "hol" and "hum", respectively. Significance thresholds: * $p < 0.05$ and ** $p < 0.001$.

			Umbusi Bog							Laukasoo Bog							Cumulative precipitation					
			Levelling				WT			Levelling				WT								
			U2	U4	$U6_{hol}$	$U6_{hum}$	U2	U4	U5	L2	L4	$L6_{hol}$	$L6_{hum}$	L2	L3	L7	Pr.1	Pr.6	Pr.9	Pr.12	Pr.15	Pr.18
Umbusi Bog	Levelling	U2	1.00																			
		U4	0.93**	1.00																		
		$U6_{hol}$	0.67**	0.81**	1.00																	
		$U6_{hum}$	0.64**	0.80**	0.98**	1.00																
	WT	U2	0.60**	0.68**	0.83**	0.79**	1.00															
		U4	0.83**	0.82**	0.78**	0.69**	0.77**	1.00														
		U5	0.80**	0.82**	0.77**	0.68**	0.79**	0.89**	1.00													
Laukasoo Bog	Levelling	L2	0.47**	0.60**	0.58**	0.55**	0.55**	0.54**	0.61**	1.00												
		L4	0.09	0.10	0.26*	0.18	0.23*	0.27*	0.37**	0.18*	1.00											
		$L6_{hol}$	0.45**	0.56**	0.83**	0.75**	0.79**	0.73**	0.70**	0.59**	0.38**	1.00										
		$L6_{hum}$	0.55**	0.71**	0.96**	0.94**	0.82**	0.71**	0.70**	0.63**	0.28*	0.89**	1.00									
	WT	L2	0.68**	0.75**	0.81**	0.73**	0.85**	0.84**	0.88**	0.71**	0.33**	0.87**	0.83**	1.00								
		L3	0.68**	0.67**	0.58**	0.49**	0.58**	0.75**	0.86**	0.62**	0.38**	0.68**	0.58**	0.85**	1.00							
		L7	0.78**	0.79**	0.61**	0.57**	0.52**	0.70**	0.82**	0.61**	0.26*	0.53**	0.56**	0.76**	0.89**	1.00						
Cumulative precipitation		Pr.1	-0.04	-0.11	0.06	-0.05	0.11	0.21*	0.12	0.01	0.19*	0.31**	0.06	0.15	0.22*	0.03	1.00					
		Pr.6	0.13	0.05	0.24*	0.12	0.37**	0.45**	0.37**	0.08	0.27*	0.55**	0.29*	0.47**	0.46**	0.20*	0.61**	1.00				
		Pr.9	0.29*	0.19*	0.32**	0.19*	0.46**	0.61**	0.54**	0.18	0.30**	0.59**	0.36**	0.58**	0.57**	0.31**	0.51**	0.90**	1.00			
		Pr.12	0.36**	0.24*	0.34**	0.20*	0.50**	0.65**	0.62**	0.23*	0.31**	0.56**	0.36**	0.62**	0.61**	0.37**	0.43**	0.78**	0.91**	1.00		
		Pr.15	0.36**	0.22*	0.31**	0.18	0.48**	0.62**	0.60**	0.24*	0.33**	0.48**	0.31**	0.59**	0.57**	0.34**	0.41**	0.69**	0.81**	0.92**	1.00	
		Pr.18	0.34**	0.23*	0.28*	0.16	0.45**	0.59**	0.60**	0.24*	0.28*	0.43**	0.27*	0.57**	0.55**	0.34**	0.39**	0.68**	0.76**	0.86**	0.94**	1.00

the preceding 18-day period was weak but statistically significant; and stronger than the correlation between WT and the precipitation sum of less than nine preceding days, which ranged from negligible to weak (Table 5). This is consistent with existing knowledge about WT and surface changes in peatlands. The difference in peat bulk density between hollows and ridges or hummocks, as well as between diplotelmic (with acrotelm) and haplotelmic parts of the bog, is the main factor facilitating a fast surface uplift response to rainfall in hollows and the diplotelmic parts of bogs. The main role in WT and surface level lowering is played by evapotranspiration combined with subsurface flow, but this is a slower process and more uniform across different vegetation complexes except for hollows where, due to the low bulk density, WT and surface height are strongly correlated.

Temporal behaviour of interferometric coherence

We had 13 consecutive interferograms (seven with 12-day and six with 6-day temporal baseline) over the study period. Umbusi reference 1 (buildings) showed minimum coherence (γ_{min}) 0.79 and maximum

Table 5. Correlations between the daily median of automatically measured peatland water table depth below surface (WT) and the cumulative daily precipitation sum (Pr.) of the preceding period of 1, 6, 9, 12, 15 and 18 days during the growing seasons (15 Apr–31 Oct) of the years 2012–2018. WT was measured relative to the peatland surface. 1041 days have been correlated. The letters "U" and "L" (together with the plot identifier) denote measurement plots along the drainage gradient in Umbusi Bog and Laukasoo Bog. Significance thresholds: * $p < 0.05$ and ** $p < 0.001$.

		Umbusi Bog			Laukasoo Bog			Cumulative precipitation					
		U2	U4	U5	L2	L3	L7	Pr.1	Pr.6	Pr.9	Pr.12	Pr.15	Pr.18
Umbusi bog	U2	1.00											
	U4	0.75**	1.00										
	U5	0.79**	0.94**	1.00									
Laukasoo bog	L2	0.76**	0.78**	0.89**	1.00								
	L3	0.61**	0.84**	0.89**	0.91**	1.00							
	L7	0.66**	0.75**	0.85**	0.89**	0.88**	1.00						
Cumulative precipitation	Pr.1	0.02	0.10*	0.09*	0.07*	0.09*	0.06	1.00					
	Pr.6	0.08*	0.23**	0.23**	0.20**	0.25**	0.13**	0.52**	1.00				
	Pr.9	0.14**	0.30**	0.30**	0.26**	0.31**	0.16**	0.45**	0.88**	1.00			
	Pr.12	0.20**	0.35**	0.36**	0.31**	0.35**	0.20**	0.37**	0.77**	0.91**	1.00		
	Pr.15	0.26**	0.38**	0.40**	0.35**	0.38**	0.23**	0.31**	0.66**	0.81**	0.93**	1.00	
	Pr.18	0.31**	0.40**	0.43**	0.38**	0.40**	0.25**	0.27**	0.59**	0.73**	0.85**	0.94**	1.00

coherence (γ_{max}) 0.97 (if the image pair of 23–29 Oct, which may be affected by snowfall, was excluded), whereas Umbusi reference 2 (road extension) had γ_{min} 0.24 and γ_{max} 0.63. Plot U4 had γ_{min} 0.29, γ_{max} 0.75 and Plot U6 had γ_{min} 0.18, γ_{max} 0.85. At Laukasoo reference 1 (junction) γ_{min} was 0.26, γ_{max} 0.83 and at reference 2 (causeway) γ_{min} was 0.19 and γ_{max} was 0.76, whereas reference 3 (building) had γ_{min} 0.86 and γ_{max} 0.98. Plot L4 had γ_{min} 0.16, γ_{max} 0.82, and Plot L6 had γ_{min} 0.46, γ_{max} 0.91.

In Umbusi, the number of image pairs that retained minimum reliable coherence ($\gamma > 0.4$) at U4, U6 and reference 2 (road extension) was 10 (out of 13), and at reference 1 (buildings) it was 12. In Laukasoo, the number of image pairs that attained $\gamma > 0.4$ was 11 at L4 but 13 at L6 and reference 3 (building). At Laukasoo references 1 (junction) and 2 (causeway), nine image pairs had $\gamma > 0.4$. In both Umbusi and Laukasoo (Figure 3 and Figure 4), the image pair of 13–25 Jul showed low coherence and moderately large bog surface subsidence, coinciding with a transition from a rainy period to a dry one. In the image pair of 11–23 Sep, coherence was reduced in all Umbusi plots after a dry period roughly three weeks long and a relatively large drop in surface elevation. Introduction of the 6-day temporal baseline starting with the image pair of 23–29 Sep coincided with higher γ values at all plots (except 23–29 Oct in Umbusi Bog).

Correlation between bog breathing and DInSAR measurements

There were considerable differences in the behaviour of DInSAR phase and coherence between the open bog, peat extraction areas and reference plots as illustrated by Figures 5, 6, A3 and A4. The radar often recorded a distinctive phase change (i.e. deformation) over the peat extraction fields along Umbusi transect 1 (illustrated by Figure 5c), which was referenced to the buildings, even though milled peat fields are characterised by compacted peat, effective drainage and relative stability. This phase change was often present even in image pairs of relatively good coherence, where it could not be caused solely by phase decorrelation (for further discussion, see Tampuu *et al*. 2021a). However, the phenomenon was not present in many of the autumn images (as illustrated by Figure 6).

The correlation between the u_{LOS} deformation estimated using the DInSAR technique and the vertical peatland surface deformations measured in situ is shown in Figure 7, where we have referenced

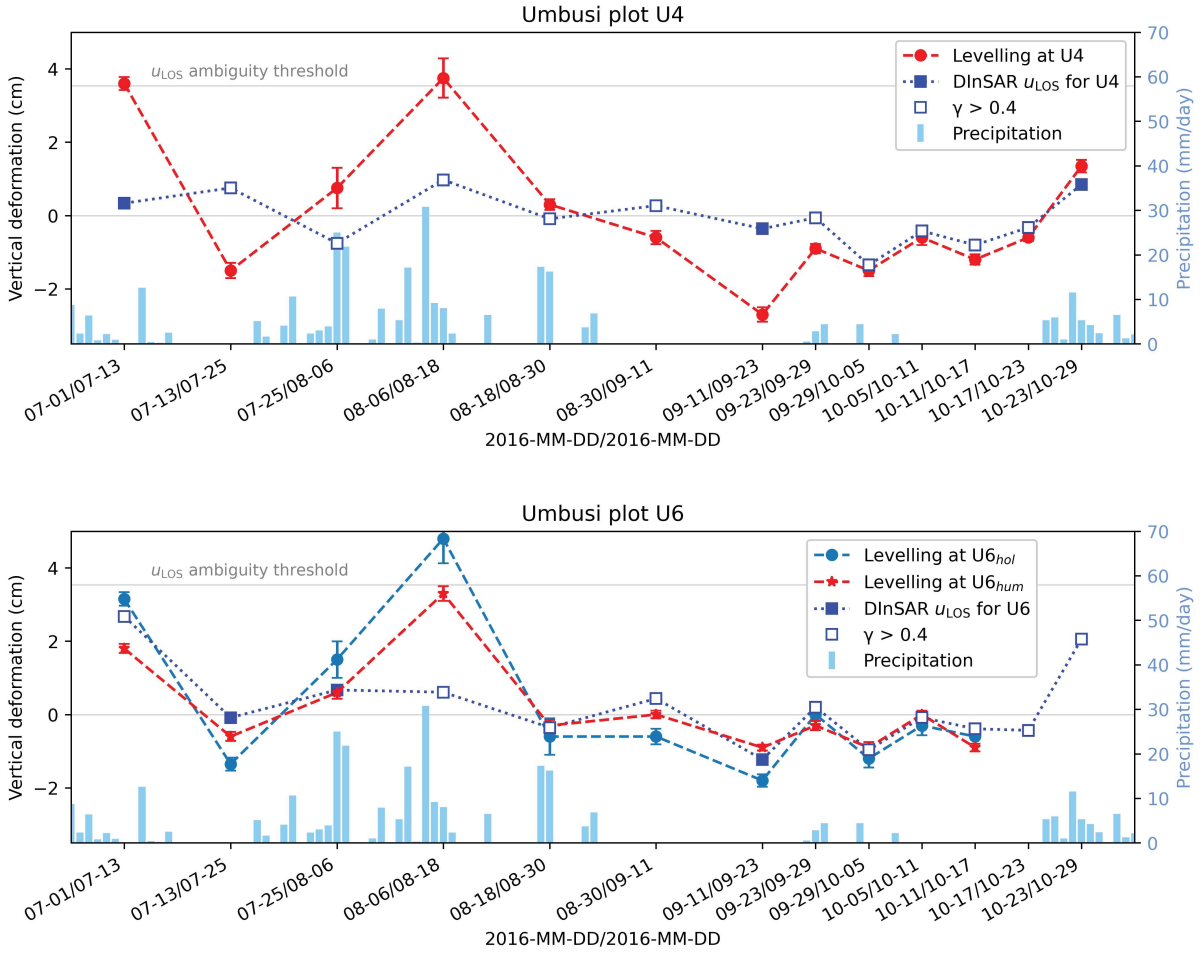

Figure 3. DInSAR line of sight deformation projected to vertical direction (u_{LOS}) (i.e. altitude change) compared to vertical surface deformation measured in situ by levelling (shown with standard deviation) between consecutive SAR acquisition dates at Plots U4 and U6 in Umbusi Bog. Levelling measurements from hollow and hummock nanotopes at U6 are denoted by the subscripts "hol" and "hum", respectively. Daily precipitation sum corresponds to the date of the second image of each pair. Coherence threshold $\gamma > 0.4$ set for the pixel corresponding to the levelling plot indicates whether the quality of the phase measurement can be trusted.

Plots U4, U6$_{hol}$ and U6$_{hum}$ to the buildings 560 m away (Umbusi reference 1). It must be remembered that the resolution of S1 (satellite) data is relatively coarse and one pixel is much larger than a single nanotope. Therefore, the backscattering response is formed at microtope level and it is not known which nanotopes dominate in the response. The Spearman's correlation coefficients (r_s) between DInSAR estimates and surface levelling measurements corresponding to the period covered by an interferogram were moderate (r_s 0.53; p-value 0.061) at U4, strong (r_s 0.85; p-value < 0.001) at U6$_{hol}$ and very strong (r_s 0. 93; p-value < 0.001) at U6$_{hum}$ (Figure 7a1–a3). We were not able to reliably detect deformations close to or more than the u_{LOS} ambiguity threshold. None of the interferograms displayed a fringe pattern, which occurs when the deformation phase jumps from +1π radian to -1π radian or vice versa, when the levelling data confirmed deformations larger than the LOS ambiguity threshold (illustrated by Figure 5b). The transects in Figure 5c are noisy but clearly do not display any phase jumps. Addition or subtraction of a phase cycle (correctly resolved ambiguity) could have improved our results (Figure 7). When referenced to the road extension (Umbusi reference 2), Plots U4, U6$_{hol}$ and U6$_{hum}$ displayed statistically insignificant negligible to weak correlation. Referencing the plots to the mean value of the active peat milling field along transect 1

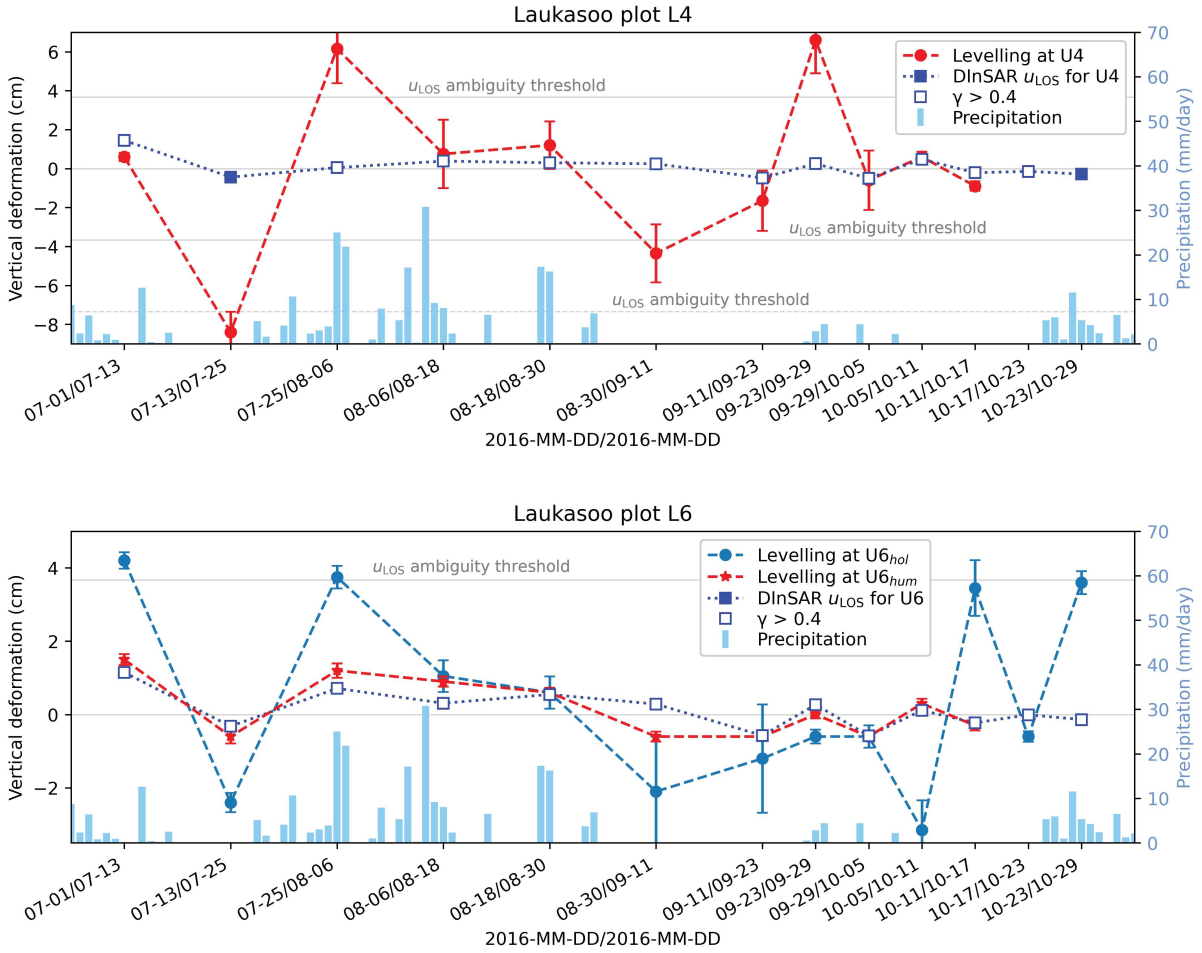

Figure 4. DInSAR line of sight deformation projected to vertical direction (u_{LOS}) (i.e. altitude change) compared to vertical surface deformation measured in situ by levelling (shown with standard deviation) between consecutive SAR acquisition dates at Plots L4 and L6 in Laukasoo Bog. Note the wider span of the y-axis for L4. Levelling measurements from hollow and hummock nanotopes at L6 are denoted by the subscripts "hol" and "hum", respectively. Daily precipitation sum corresponds to the date of the second image of each pair. Coherence threshold $\gamma > 0.4$ set for the pixel corresponding to the levelling plot indicates whether the quality of the phase measurement can be trusted.

resulted in statistically insignificant negligible and weak correlations at U4 and U6$_{hol}$, respectively, and a near to significant moderate correlation (r_s 0.58; p-value 0.063) at U6$_{hum}$. Umbusi plots referenced to the mean value of the active peat milling field along transect 2 gave negligible correlations at U4 and U6$_{hol}$ and a weak correlation at U6$_{hum}$, although all of the correlations were not statistically significant.

When Laukasoo levelling plots were referenced to the building slightly less than one kilometre away (Laukasoo reference 3), the correlation between the DInSAR results and surface levelling measurements corresponding to the period covered by an interferogram was statistically insignificant and weak to moderate for L4 and L6$_{hol}$. At Plot L6$_{hum}$, the correlation was statistically significant and strong (r_s 0.82; p-value 0.002) (Figure 7b1–b3). The plots in Laukasoo Bog, when referenced to the junction (Laukasoo reference 1) or to the causeway (Laukasoo reference 2), displayed negligible negative or positive and mainly statistically insignificant correlations. When referenced to the mean value of the abandoned peat milling field along transect 1, Plots L4, L6$_{hol}$ and L6$_{hum}$ displayed statistically insignificant weak correlation coefficients. Referencing the levelling plots to the mean value for the active peat milling field along transect 2 gave statistically insignificant negligible or weak negative correlations.

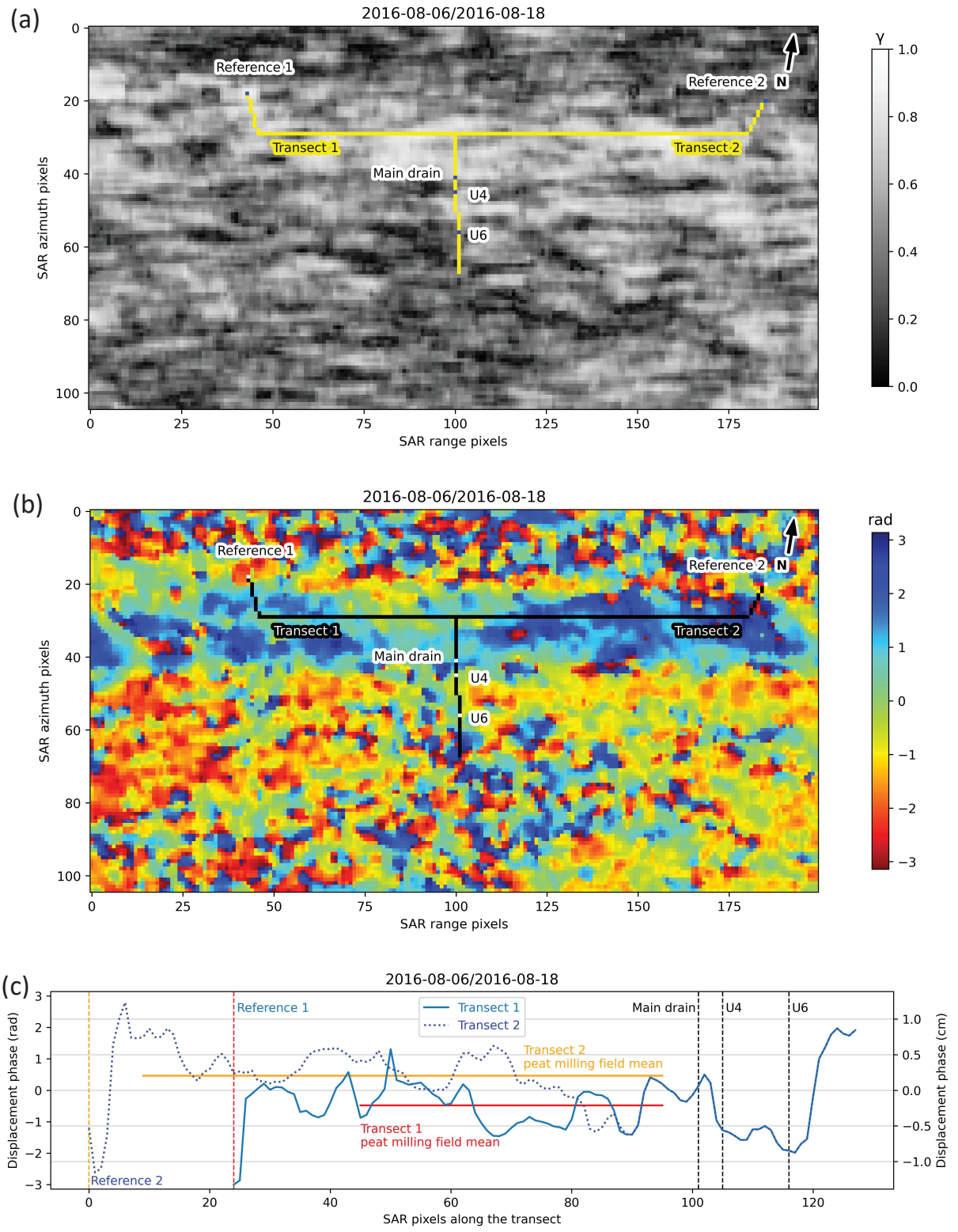

Figure 5. Umbusi Bog: InSAR coherence γ (a) and phase (b) images and radar line of sight deformation along the virtual transects (c) in radar coordinates for the image pair of 06–18 Aug 2016. Stable reference points used in DInSAR processing and the plots (U4 and U6; ground levelling data available) used in validation of DInSAR deformation estimates are indicated. The geographic coordinates of the scene are shown in Figure 1.

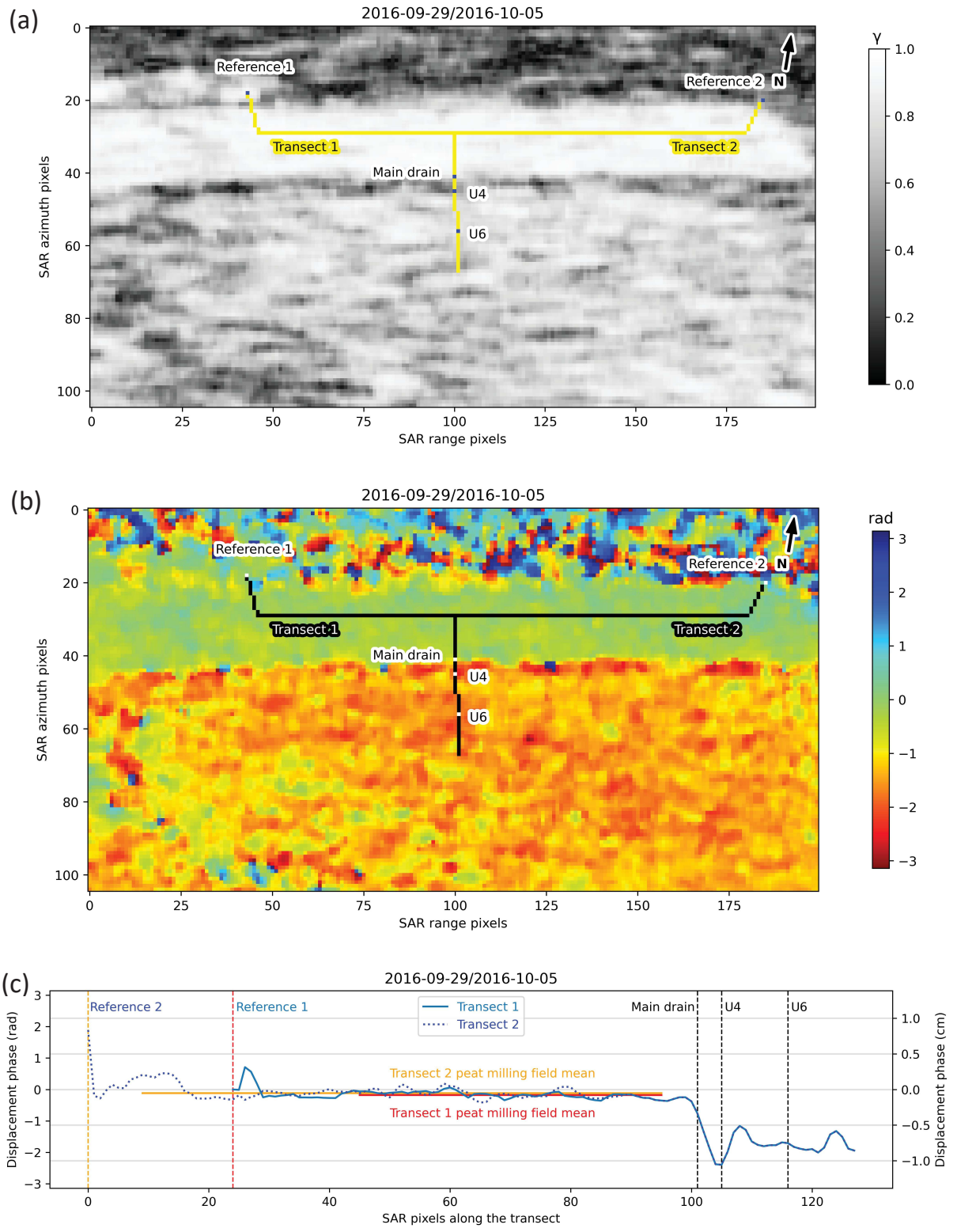

Figure 6. Umbusi Bog: InSAR coherence γ (a) and phase (b) images and radar line of sight deformation along the virtual transects (c) in radar coordinates for the image pair of 29 Sep–05 Oct 2016. Stable reference points used in DInSAR processing and the plots (U4 and U6; ground levelling data available) used in validation of DInSAR deformation estimates are indicated. The geographic coordinates of the scene are shown in Figure 1.

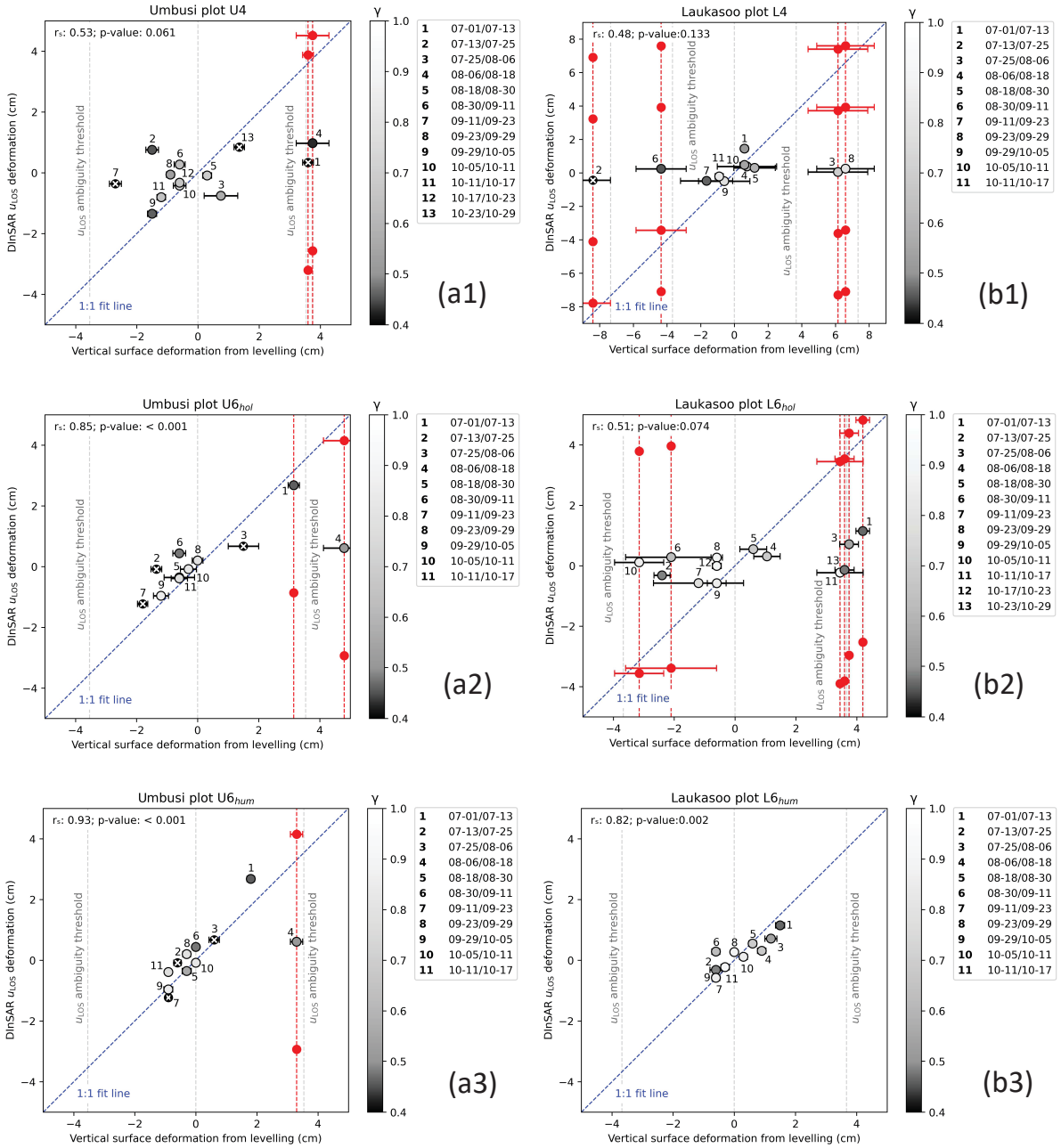

Figure 7. Correlations (r_s) between the vertical surface deformation measured in situ by levelling (x-axis, shown with standard deviation) and DInSAR line of sight deformation projected to vertical dimension (u_{LOS}) at (a1–a3) Umbusi plots U4, U6$_{hol}$ (hollow) and U6$_{hum}$ (hummock) and (b1–b3) Laukasuo plots L4, L6$_{hol}$ (hollow) and L6$_{hum}$ (hummock). A white X on black background marks a data point of DInSAR coherence $\gamma > 0.4$ (indicating unreliable phase estimate). Red points represent u_{LOS} values if a phase cycle is added/subtracted in the cases where the in-situ value is close to the Sentinel-1 u_{LOS} ambiguity threshold. Notice the wider span of the x-axis in (b1).

The amplitude of bog breathing in the observation periods of 6–12 days differ among nanotopes but usually lie in the range of the u_{LOS} ambiguity threshold (3.54 cm in Umbusi and 3.67 cm in Laukasoo). Only the natural hummock nanotope displayed surface deformations between the radar acquisition dates that were consistently less than the u_{LOS} ambiguity threshold (Figures 3–4 and Figure 7).

DISCUSSION

Bog breathing and its spatiotemporal variability

We studied bog breathing along the gradient of decreasing drainage influence in two raised bogs continuously, using automatic levelling devices exploiting the travel time of ultrasound between the sensor and the ground. Automated systems have been recommended for monitoring bog breathing (Marshall *et al*. 2022). In other peatland environments, the use of extensometers (Van Asselen *et al*. 2020, Conroy *et al*. 2022) and cameras (Evans *et al*. 2021) has recently been demonstrated. We used the transect-based approach to gauge not only how bog breathing proceeds through time, but also how it develops along the drainage gradient. We also studied the behaviour of different nanotopes along the transect; most significantly, we compared the dynamics of a natural hollow and a hummock just two metres apart. The variability of bog breathing in blanket bogs in the UK was recently studied by Marshall *et al*. (2022) who showed the interior parts of blanket bogs being the most dynamic and undergoing large surface deformation in extreme drought conditions. Additionally, we have presented a preliminary analysis of how the mechanisms underlying bog breathing (in this study precipitation and WT in regard to nanotopes) (Roulet 1991, Kellner & Halldin 2002, Morton & Heinemeyer 2019) are correlated to the recorded surface motion.

We measured the range of bog breathing in two raised bogs as 11.6–14.7 cm at natural and disturbed hollow nanotopes and 6.9–7.5 cm at natural hummock nanotopes during the growing season of 2016. The haplotelmic nanotopes oscillated in the range 9.5–11.6 cm. Our levelling measurements agree with preceding in situ research by others. A literature review by Fritz (2006) found that bog breathing amounts to 2.6–11 cm in natural bogs (11 plots from 9 studies) and 0.7–13 cm in disturbed peatlands (14 plots in 12 studies). Howie & Hebda (2018) recorded a multiyear average surface oscillation of 11.7 cm at plots in natural raised bog, whereas disturbed plots had a mean of 9.1 cm. Marshall *et al*. (2022) measured an inter-seasonal range of 3–12 cm in the interior part of a low-lying blanket bog.

We recorded the largest surface elevation changes over a 1-day period in a disturbed hollow nanotope: up to 6.6 cm of uplift and up to 7.8 cm of subsidence. The short-term vertical surface changes in hummocks were modest and below the Sentinel-1 LOS ambiguity threshold (2.77 cm) in any given 6-day period. Glaser *et al*. (2004) observed oscillations at a raised bog plot that exceeded 20 cm over a period of four hours. The time needed for the peat matrix to equilibrate with the changed WT may range from hours to days (Fritz *et al*. 2008).

Bog breathing is generally smallest, and rapid surface movements are rare, when the peat has become uniformly saturated with rainwater. The surface elevation changes in different nanotopes are most uniform for periods of very dry or fully water-saturated peat conditions. Regarding fully saturated peat, when pores are filled with rainwater up to the surface, any excess rainwater simply flows away across the peat surface and through the acrotelm (Holden *et al*. 2004). The surface fluctuations are caused by relatively uniform changes in WT and the magnitudes of change in hollows and hummocks harmonise (illustrated by $U6_{hol}$ and $U6_{hum}$ in late September and October; Figure 3). Regarding dry peat, the rainwater pours freely through the pores of the upper peat layers without being trapped there and the surface fluctuations depend solely on the uniform expansion or shrinkage of the lower-lying layers (Evans *et al*. 1999). The amplitude of bog breathing is largest during periods when the peat is nearly saturated with water. The water-filled pore space is a poor conductor of water, therefore the surface fluctuations become determined by the amount of rainfall and where the rainwater accumulates on the peat surface (Kellner & Halldin 2002). Consequently, the disparity in the magnitude of bog breathing in hollows and hummocks is considerable (illustrated by $L6_{hol}$ and $L6_{hum}$ in autumn; Figure 4). Accordingly, hollows and hummocks fluctuated at different magnitudes during most of the summer (Plot U6 in Figure 3, Plot L6 in Figure 4).

Perspectives for DInSAR in northern raised bogs

Our results show that DInSAR u_{LOS} deformation estimates correlate moderately to strongly with bog breathing measured in situ. The highest correlations were recorded in natural hummock nanotopes, which are especially suitable for applying DInSAR because their surface fluctuations in any given 6-day period were always below the LOS ambiguity threshold.

Thus, despite under-estimating the larger surface height changes, the bog breathing estimates from conventional DInSAR contain a useful deformation signal. However, it was only when buildings were used as stable reference points for the DInSAR phase measurements that the correlation between remotely estimated and in situ measured surface deformation values became strong and statistically significant. Using causeways as reference points gave only a statistically insignificant weak correlation. This indicates that further complications can be expected when using C-band conventional DInSAR in peatlands which are located in remote areas.

A useful deformation signal is also contained in advanced DInSAR time series, as demonstrated by Tampuu *et al*. (2022) using the method of Ansari *et al*. (2018). This is in accordance with Marshall *et al*. (2022) who showed, using an advanced DInSAR time series approach by Cigna & Sowter (2017), that despite under-estimation of the magnitude of oscillation, the timing of peaks and valleys in the time series and the direction of change were mostly correct. Even without precise bog breathing magnitudes, that information could allow a wide scale assessment of the status of peatlands, as demonstrated recently (Alshammari *et al*. 2020, Bradley *et al*. 2022, Islam *et al*. 2022).

Our approach to overcoming the ambiguity issue and deriving precise magnitudes of peatland surface elevation changes was twofold. First, limiting the time interval between radar images to the minimum available, and thereby reducing the magnitude of surface displacement that had to be sensed (Alshammari *et al*. 2018), aimed to eliminate the need for unwrapping. Secondly, establishing the virtual transect stretching from stable ground to the levelling plots helped us to predict the dominant direction of elevation change along the transect, which we presumed could guide phase ambiguity resolution when unwrapping was needed. However, none of the interferograms displayed fringes (recognisable phase jumps) when the levelling data confirmed deformations larger than the LOS ambiguity threshold, and we were not able to reliably estimate such deformations.

On one hand, the loss of DInSAR coherence at the bog margins, caused by the tree cover, makes a phase jump in a marginal bog area invisible to C-band (Tampuu *et al*. 2020). On the other hand, even the haplotelmic plots only 15 m from the drainage ditch experienced bog breathing of up to 9.5 cm and rapid surface displacements that exceeded the LOS ambiguity threshold in just a single day. Thus, Sentinel-1 pixels with spatial resolution around 3 m × 22 m in IW mode (CLS 2016) may be too large to capture the deformation gradient. The maximum detectable deformation gradient is one fringe per pixel (Massonnet & Feigl 1998, Rosen *et al*. 2000), being affected also by DInSAR coherence and the number of looks (Jiang *et al*. 2011). We used a phase filtering window with a ~40 m footprint on the ground. Alshammari *et al*. (2018) and Marshall *et al*. (2022) used multilooked pixels with a side of ~80 m and an advanced DInSAR method, which allows estimates to be retrieved also in wooded peatland areas (Alshammari *et al*. 2018). Future research could consider working with unfiltered unmultilooked pixels to preserve the maximum spatial resolution and avoid the possibility of averaging over the deformation gradient occurring across such a limited spatial extent.

To tackle the ambiguity issue, future research should consider the introduction of contextual information, e.g. temperature, precipitation and evapotranspiration (Roulet 1991, Lhosmot *et al*. 2021) to guide unwrapping, following the work by Heuff & Hanssen (2020) and Conroy *et al*. (2022) on peatland grasslands. This could make C-band DinSAR reliable also in estimating larger changes, as we have demonstrated up to moderate statistically significant relationships between precipitation, WT and bog surface height. Alternatively, Zhou *et al*. (2010) and Zhou (2013) have recommended using longer wavelength radar, which would mitigate the unwrapping problem by allowing the surface displacement to fit into one phase cycle (Hoyt *et al*. 2020) and also by increasing penetration through the forest cover (Wei & Sandwell 2010, Hoyt *et al*. 2020, Umarhadi *et al*. 2021) at bog margins. The imminent L-band (wavelength 24 cm) missions NISAR (NASA 2021) and ROSE-L (Davidson & Furnell 2021) could make this possible.

Importance of the availability of levelling measurements to verify DInSAR deformation estimates

The magnitudes of bog breathing recorded by us and reported in the literature indicate the possibility that the rather modest DInSAR bog surface deformation estimates that have not been validated with ground levelling data could be underestimates (Zhou *et al*. 2010, Zhou 2013, Cigna *et al*. 2014, Cigna & Sowter 2017, Fiaschi *et al*. 2019, Alshammari *et al*. 2020, Tampuu *et al*. 2020, Bradley *et al*. 2022). The underestimation, shown in our comparison with ground levelling data, has been previously confirmed by Alshammari *et al.* (2018), and by Marshall *et al*. (2022) under drought conditions in the most intact

parts of a blanket bog. We have shown that underestimation can occur in any microtope within a raised bog under normal climatic conditions.

C-band DInSAR studies in permafrost regions are also characterised by a lack of in situ ground validation data (Iwahana *et al*. 2021), posing a similar question of reliability. For example, the foundational DInSAR study by Liu *et al*. (2010) measured subsidence of 1–4 cm in tundra during the thawing season, whereas Iwahana *et al*. (2021) reported average seasonal thaw settlements of 5.8–14.3 cm based on in situ measurements. De la Barreda-Bautista *et al*. (2022) measured maximum subsidence of 25 cm in permafrost peatlands using digital elevation models (DEMs) derived from multispectral and true colour RGB imagery captured from Unmanned Aerial Vehicles (UAVs), whereas the maximum subsidence detected by DInSAR was 1.5 cm.

We highlight that the ability of DInSAR to accurately estimate bog breathing is limited, and we were not able to detect estimation errors by inspection of the DInSAR data alone. The errors were found only by comparison with ground-based validation data. As it is uncertain whether, when and where peatland surface height changes can be presumed to remain within a convenient range for C-band observations, we emphasise the need for caution when interpreting DInSAR bog breathing estimates without ground validation. The uncertainty regarding conditions under which sufficiently small surface height changes can be presumed has also been demonstrated in blanket bogs by Marshall *et al*. (2022). Also, the proportion of hummocks and ridges versus hollows within microtopes, and consequently within SAR pixels, varies between different parts of a bog and between bogs, complicating the process of relating SAR data to ground-based data.

An aspect not covered in this study is what exactly governs C-band radar backscatter in peatlands, which goes beyond merely estimating the proportion of nanotopes in an image pixel or averaging window (Morrison 2013). We found that DInSAR estimates correlated better to ground-based measurements on hummocks than in hollows if both were found in an image pixel. However, it is not known how that reflects the possible predominance of signal from hummocks in backscatter, the areal dominance of hummocks in a particular pixel, or the struggle of DInSAR to measure larger changes (Marshall *et al*. 2022). The question of how faithfully in situ point measurements can represent surface deformations across the much larger areas of SAR pixels is a concern (Alshammari *et al*. 2018, Alshammari *et al*. 2020) that is yet to be resolved (Marshall *et al*. 2022).

ACKNOWLEDGEMENTS

This study formed part of a PhD project supported by the European Union from the European Regional Development Fund. The research was funded by Estonian Environmental Investment Centre grants SLOOM12006 and SLOOM14103, Estonian State Forest Management Centre grant LLTOM17250, and national scholarship program Kristjan Jaak which is funded and managed by the Archimedes Foundation in collaboration with the Ministry of Education and Research (Estonia). The authors thank Karsten Kretschmer (DLR) for helping with Python, Philip Conroy for giving a native speaker's touch to the manuscript, and the SarProz team for their excellent software and extremely flexible student licensing.

AUTHOR CONTRIBUTIONS

Conceptualisation and general design of the field studies: AK; DInSAR methodology: TT, JP; field data and data curation: AK, MK, TT; formal analysis: TT, AK, JP; resources and supervision of the research: AK, JP, FDZ; writing - preparation of first draft: TT; writing - review and editing: JP, AK, FDZ; funding acquisition: AK.

REFERENCES

Alekseychik, P., Korrensalo, A., Mammarella, I., Launiainen, S., Tuittila, E.S., Korpela, I. Vesala, T. (2021) Carbon balance of a Finnish bog: temporal variability and limiting factors based on 6 years of eddy-covariance data. *Biogeosciences*, 18(16), 4681–4704.

Alshammari, L., Large, D.J., Boyd, D.S., Sowter, A., Anderson, R., Andersen, R., Marsh, S. (2018) Long-term peatland condition assessment via surface motion monitoring using the ISBAS DInSAR technique over the Flow Country, Scotland. *Remote Sensing*, 10(7), 1103, 24 pp.

Alshammari, L., Boyd, D.S., Sowter, A., Marshall, C., Andersen, R., Gilbert, P., Marsh, S. Large, D.J. (2020) Use of surface motion characteristics determined by InSAR to assess peatland condition. *Journal of Geophysical Research: Biogeosciences*, 125(1): e2018JG004953, 15 pp.

Ansari, H., De Zan, F., Bamler, R. (2018) Efficient phase estimation for interferogram stacks. *IEEE Transactions on Geoscience and Remote Sensing*, 56(7), 4109–4125.

Bamler, R., Hartl, P. (1998) Synthetic aperture radar

interferometry. *Inverse Problems*, 14(4), R1–R54.

Bekaert, D.P.S., Walters, R.J., Wright, T.J., Hooper, A.J., Parker, D.J. (2015) Statistical comparison of InSAR tropospheric correction techniques. *Remote Sensing of Environment*, 170, 40–47.

Berardino, P., Fornaro, G., Lanari, R., Sansosti, E. (2002) A new algorithm for surface deformation monitoring based on small baseline differential SAR interferograms. *IEEE Transactions on Geoscience and Remote Sensing*, 40(11), 2375–2383.

Biggs, J., Wright, T.J. (2020) How satellite InSAR has grown from opportunistic science to routine monitoring over the last decade. *Nature Communications*, 11(1), 3863, 4 pp.

Blodau, C. (2002) Carbon cycling in peatlands – A review of processes and controls. *Environmental Reviews*, 10(2), 111–134.

Bradley, A.V., Andersen, R., Marshall, C., Sowter, A., Large, D.J. (2022) Identification of typical ecohydrological behaviours using InSAR allows landscape-scale mapping of peatland condition. *Earth Surface Dynamics Discussions*, 10(2), 261–2771.

Braun, A., Veci, L. (2020) *TOPS Interferometry Tutorial*. Sentinel-1 Toolbox, ESA / Skywatch Space Applications Inc., New York. Online at: http://step.esa.int/docs/tutorials/S1TBX%20TOPSAR%20Interferometry%20with%20Sentinel-1%20Tutorial_v2.pdf, accessed 01 Oct 2020.

Cigna, F., Sowter, A. (2017) The relationship between intermittent coherence and precision of ISBAS InSAR ground motion velocities: ERS-1/2 case studies in the UK. *Remote Sensing of Environment*, 202, 177–198.

Cigna, F., Sowter, A., Jordan, C.J., Rawlins, B.G. (2014) Intermittent Small Baseline Subset (ISBAS) monitoring of land covers unfavourable for conventional C-band InSAR: proof-of-concept for peatland environments in North Wales, UK. In: *SAR Image Analysis, Modeling, and Techniques XIV*, SPIE Proceedings Volume 9243, International Society for Optics and Photonics, 924305.

CLS (2016) Sentinel-1 Product Definition, Issue 2.7, S1-RS-MDA-52-7440. Collecte Localisation Satellites (CLS), European Space Agency (ESA). Online at: https://dragon3.esa.int/web/sentinel/user-guides/sentinel-1-sar/document-library/-/asset_publisher/1dO7RF5fJMbd/content/sentinel-1-product-definition, accessed 08 Nov 2021.

Conroy, P., van Diepen, S.A.N, van Asselen, S., Erkens, G., van Leijen, F.J., Hanssen, R.F. (2022) Probabilistic estimation of InSAR displacement phase guided by contextual information and artificial intelligence. *IEEE Transactions on Geoscience and Remote Sensing*, 60, 5234611, 11 pp.

Crosetto, M., Monserrat, O., Cuevas-González, M., Devanthéry, N., Crippa, B. (2016) Persistent scatterer interferometry: A review. *ISPRS Journal of Photogrammetry and Remote Sensing*, 115, 78–89.

Davidson, M.W.J., Furnell, R. (2021) ROSE-L: Copernicus L-Band SAR Mission. In: *IGARSS 2021*, 2021 IEEE International Geoscience and Remote Sensing Symposium, IEEE, 872–873.

De la Barreda-Bautista, B., Boyd, D.S., Ledger, M., Siewert, M.B., Chandler, C., Bradley, A.V., Gee, D., Large, D.J., Olofsson, J., Sowter, A., Sjogersten, S. (2022) Towards a monitoring approach for understanding permafrost degradation and linked subsidence in arctic peatlands. *Remote Sensing*, 14(3), 444, 19 pp.

Dise, N.B. (2009) Peatland response to global change. *Science*, 326(5954), 810–811.

Esch, C., Köhler, J., Gutjahr, K., Schuh, W.D. (2019) On the analysis of the phase unwrapping process in a D-InSAR stack with special focus on the estimation of a motion model. *Remote Sensing*, 11(19), 2295, 20 pp.

Estonian Environment Agency (2021) Weather, Observation data: daily data. Online at: http://www.ilmateenistus.ee/ilm/ilmavaatlused/vaatlusandmed/oopaevaandmed/?lang=en, accessed 14 Sep 2021.

Estonian Environment Agency (2023) Climate: Climate normals: Temperature, Precipitation etc. Online at: https://www.ilmateenistus.ee/kliima/kliimanormid/ohutemperatuur/?lang=en, accessed 29 Apr 2023.

Evans, C.D., Callaghan, N., Jaya, A., Grinham, A., Sjogersten, S., Page, S.E., Harrison, M.E., Kusin, K., Kho, L.K., Ledger, M., Evers, S., Mitchell Z., Williamson J., Radbourne A.D., Jovani-Sancho, A.J. (2021) A novel low-cost, high-resolution camera system for measuring peat subsidence and water table dynamics. *Frontiers in Environmental Science*, 9, 630752, 18 pp.

Evans, M.G., Burt, T.P., Holden, J., Adamson, J.K. (1999) Runoff generation and water table fluctuations in blanket peat: evidence from UK data spanning the dry summer of 1995. *Journal of Hydrology*, 221(3–4), 141–160.

Ferretti, A., Prati, C., Rocca, F. (2001) Permanent scatterers in SAR interferometry. *IEEE Transactions on Geoscience and Remote Sensing,* 39(1), 8–20.

Ferretti, A., Monti-Guarnieri, A., Prati, C., Rocca, F., Massonnet, D. (2007) *InSAR Principles:*

Guidelines for SAR Interferometry Processing and Interpretation. Fletcher, K. (ed.), ESA Publications, Noordwijk, The Netherlands, 48 pp.

Fiaschi, S., Holohan, E.P., Sheehy, M., Floris, M. (2019) PS-InSAR analysis of Sentinel-1 data for detecting ground motion in temperate oceanic climate zones: a case study in the Republic of Ireland. *Remote Sensing*, 11(3), 348, 30 pp.

Foster, J., Brooks, B., Cherubini, T., Shacat, C., Businger, S., Werner, C.L. (2006) Mitigating atmospheric noise for InSAR using a high resolution weather model. *Geophysical Research Letters*, 33(16), L16304, 5 pp.

Fritz, C. (2006) *Surface Oscillation in Peatlands: How Variable and Important Is It?* Master's Thesis, University of Waikato, Hamilton, New Zealand, 119 pp.

Fritz, C., Campbell, D.I., Schipper, L.A. (2008) Oscillating peat surface levels in a restiad peatland, New Zealand—magnitude and spatiotemporal variability. *Hydrological Processes*, 22(17), 3264–3274.

Fuhrmann, T., Garthwaite, M.C. (2019) Resolving three-dimensional surface motion with InSAR: Constraints from multi-geometry data fusion. *Remote Sensing*, 11(3), 241, 21 pp.

Glaser, P.H., Chanton, J.P., Morin, P., Rosenberry, D.O., Siegel, D.I., Ruud, O., Chasar, L.I., Reeve, A.S. (2004) Surface deformations as indicators of deep ebullition fluxes in a large northern peatland. *Global Biogeochemical Cycles*, 18(1), GB1003, 15 pp.

Goldstein, R.M., Werner, C.L. (1998) Radar interferogram filtering for geophysical applications. *Geophysical Research Letters*, 25(21), 4035–4038.

Gorham, E. (1991) Northern peatlands: role in the carbon cycle and probable responses to climatic warming. *Ecological Applications*, 1(2), 182–195.

Heikurainen, L., Päivänen, J., Seppälä, K. (1964) Ground water table and water content in peat soil. *Acta Forestalia Fennica*, 77, 1–18.

Heuff, F.M., Hanssen, R.F. (2020) InSAR phase reduction using the Remove-Compute-Restore method. In: *IGARSS 2020*, 2020 IEEE International Geoscience and Remote Sensing Symposium, IEEE, 786–789.

Holden, J., Chapman, P.J., Labadz, J.C. (2004) Artificial drainage of peatlands: hydrological and hydrochemical process and wetland restoration. *Progress in Physical Geography*, 28(1), 95–123.

Howie, S.A., Hebda, R.J. (2018) Bog surface oscillation (mire breathing): A useful measure in raised bog restoration. *Hydrological Processes*, 32(11), 1518–1530.

Hoyt, A.M., Chaussard, E., Seppalainen, S.S., Harvey, C.F. (2020) Widespread subsidence and carbon emissions across Southeast Asian peatlands. *Nature Geoscience*, 13(6), 435–440.

Islam, M.T., Bradley, A.V., Sowter, A., Andersen, R., Marshall, C., Long, M., Bourke, M.C., Connolly, J., Large, D.J. (2022) Potential use of APSIS-InSAR measures of the range of vertical surface motion to improve hazard assessment of peat landslides. *Mires and Peat*, 28, 21, 19 pp.

Iwahana, G., Busey, R.C., Saito, K. (2021) Seasonal and interannual ground-surface displacement in intact and disturbed tundra along the Dalton Highway on the North Slope, Alaska. *Land*, 10(1), 22, 18 pp.

Jiang, J., Lohman, R.B. (2021) Coherence-guided InSAR deformation analysis in the presence of ongoing land surface changes in the Imperial Valley, California. *Remote Sensing of Environment*, 253, 112160, 19 pp.

Jiang, M., Li, Z.W., Ding, X.L., Zhu, J.J., Feng, G.C. (2011) Modeling minimum and maximum detectable deformation gradients of interferometric SAR measurements. *International Journal of Applied Earth Observation and Geoinformation*, 13(5), 766–777.

Kellner, E., Halldin, S. (2002) Water budget and surface-layer water storage in a *Sphagnum* bog in central Sweden. *Hydrological Processes*, 16(1), 87–103.

Kull, A. (2016) *Soode ökoloogilise funktsionaalsuse tagamiseks vajalike puhvertsoonide määratlemine pikaajaliste häiringute leviku piiramiseks või leevendamiseks, II etapp* (*Defining the Buffer Zones Necessary to Ensure the Ecological Functionality of Peatlands to Limit or Mitigate the Spread of Long-term Disturbances, Stage II*). Report of the Targeted Financing Agreement 8286 SFL nr 3-2_15/835-14/2014 aruanne, 183 pp. (in Estonian). Online at: https://ainkull.wixsite.com/sood/aruanne, accessed 29 Apr 2023.

Lees, K.J., Quaife, T., Artz, R.R.E., Khomik, M., Clark, J.M. (2018) Potential for using remote sensing to estimate carbon fluxes across northern peatlands–A review. *Science of the Total Environment*, 615, 857–874.

Leifeld, J., Menichetti, L. (2018) The underappreciated potential of peatlands in global climate change mitigation strategies. *Nature Communications*, 9(1), 1071, 7 pp.

Lhosmot, A., Collin, L., Magnon, G., Steinmann, M., Bertrand, C., Stefani, V., Toussaint, M.L., Bertrand, G. (2021) Restoration and meteorological variability highlight nested water

supplies in middle altitude/latitude peatlands: Towards a hydrological conceptual model of the Frasne peatland, Jura Mountains, France. *Ecohydrology*, 14(6), e2315, 16 pp.

Lidberg, M., Johansson, J.M., Scherneck, H.G., Milne, G.A. (2010) Recent results based on continuous GPS observations of the GIA process in Fennoscandia from BIFROST. *Journal of Geodynamics*, 50(1), 8–18.

Lindsay, R. (2010). *Peatbogs and Carbon: a Critical Synthesis to Inform Policy Development in Oceanic Peat Bog Conservation and Restoration in the Context of Climate Change*. Environmental Research Group, University of East London, London, UK, 315 pp.

Liu, L., Zhang, T., Wahr, J. (2010) InSAR measurements of surface deformation over permafrost on the North Slope of Alaska. *Journal of Geophysical Research: Earth Surface*, 115, F03023, 14 pp.

Marshall, C., Sterk, H.P., Gilbert, P.J., Andersen, R., Bradley, A.V., Sowter, A., Marsh, S., Large, D.J. (2022) Multiscale variability and the comparison of ground and satellite radar based measures of peatland surface motion for peatland monitoring. *Remote Sensing,* 14(2), 336, 22 pp.

Massonnet, D., Feigl, K.L. (1998) Radar interferometry and its application to changes in the Earth's surface. *Reviews of Geophysics*, 36(4), 441–500.

Mohammadimanesh, F., Salehi, B., Mahdianpari, M., Brisco, B., Motagh, M. (2018) Multi-temporal, multi-frequency, and multi-polarization coherence and SAR backscatter analysis of wetlands. *ISPRS Journal of Photogrammetry and Remote Sensing*, 142, 78–93.

Morishita, Y., Hanssen, R.F. (2015) Deformation parameter estimation in low coherence areas using a multisatellite InSAR approach. *IEEE Transactions on Geoscience and Remote Sensing,* 53(8), 4275–4283.

Morrison, K. (2013) Mapping subsurface archaeology with SAR. *Archaeological Prospection*, 20(2), 149–160.

Morton, P.A., Heinemeyer, A. (2019) Bog breathing: the extent of peat shrinkage and expansion on blanket bogs in relation to water table, heather management and dominant vegetation and its implications for carbon stock assessments. *Wetlands Ecology and Management*, 27(4), 467–482.

NASA (2021) Quick Facts. NASA-ISRO SAR Mission (NISAR) website, NASA Jet Propulsion Laboratory (JPL), Pasadena CA, USA. Online at: https://nisar.jpl.nasa.gov/mission/quick-facts/, accessed 09 Nov 2021.

Nichols, J.E., Peteet, D.M. (2019) Rapid expansion of northern peatlands and doubled estimate of carbon storage. *Nature Geoscience*, 12(11), 917–921.

Novellino, A., Cigna, F., Brahmi, M., Sowter, A., Bateson, L., Marsh, S. (2017) Assessing the feasibility of a national InSAR ground deformation map of Great Britain with Sentinel-1. *Geosciences*, 7(2), 19, 14 pp.

Ojanen, P., Minkkinen, K., Alm, J., Penttilä, T. (2010) Soil–atmosphere CO_2, CH_4 and N_2O fluxes in boreal forestry-drained peatlands. *Forest Ecology and Management*, 260(3), 411–421.

Osmanoğlu, B., Sunar, F., Wdowinski, S., Cabral-Cano, E. (2016) Time series analysis of InSAR data: Methods and trends. *ISPRS Journal of Photogrammetry and Remote Sensing*, 115, 90–102.

Paal, J., Jürjendal, I., Suija, A., Kull, A. (2016) Impact of drainage on vegetation of transitional mires in Estonia. *Mires and Peat*, 18, 02, 19 pp.

Perissin, D. (2021) *SARPROZ©: The SAR PROcessing tool by periZ*. Online at: https://www.sarproz.com/, accessed 14 Sep 2021.

Python Software Foundation (2021) *Python* website. Online at: https://www.python.org/, accessed 15 Sep 2021.

Rosen, P.A., Hensley, S., Joughin, I.R., Li, F.K., Madsen, S.N., Rodriguez, E., Goldstein, R.M. (2000) Synthetic aperture radar interferometry. *Proceedings of the IEEE*, 88(3), 333–382.

Roulet, N.T. (1991) Surface level and water table fluctuations in a subarctic fen. *Arctic and Alpine Research*, 23(3), 303–310.

Shapiro, S.S., Wilk, M.B. (1965) An analysis of variance test for normality (complete samples). *Biometrika*, 52(3/4), 591–611.

Spearman, C. (1904) The proof and measurement of association between two things. *American Journal of Psychology*, 15(1), 72–101.

Strack, M., Kellner, E., Waddington, J.M. (2006) Effect of entrapped gas on peatland surface level fluctuations. *Hydrological Processes*, 20(17), 3611–3622.

Tampuu, T. (2022) *Synthetic Aperture Radar Interferometry as a Tool for Monitoring the Dynamics of Peatland Surface*. PhD thesis, University of Tartu, Tartu, Estonia, 166 pp.

Tampuu, T., Praks, J., Uiboupin, R., Kull, A. (2020) Long term interferometric temporal coherence and DInSAR phase in Northern Peatlands. *Remote Sensing*, 12(10), 1566, 22 pp.

Tampuu, T., Praks, J., De Zan, F., Kohv, M., Kull, A. (2021a) Towards assessment of bog breathing

with Sentinel-1 Differential InSAR. In: *IPC2021: 16th International Peatland Congress, Oral Presentations*, Publicon PCO, Tartu, Estonia, 472–478. Online at: IPC 2021 proceedings_oral presentations_f.pdf (publicon.ee), accessed 12 May 2023.

Tampuu, T., Praks, J., Kull, A., Uiboupin, R., Tamm, T., Voormansik, K. (2021b) Detecting peat extraction related activity with multi-temporal Sentinel-1 InSAR coherence time series. *International Journal of Applied Earth Observation and Geoinformation*, 98, 102309, 11 pp.

Tampuu, T., De Zan, F., Shau, R., Praks, J., Kohv, M., Kull, A. (2022) Can bog breathing be measured by synthetic aperture radar interferometry. In: *IGARSS 2022*, IEEE International Geoscience and Remote Sensing Symposium, IEEE, 16–19.

Touzi, R., Lopes, A., Bruniquel, J., Vachon, P.W. (1999) Coherence estimation for SAR imagery. *IEEE Transactions on Geoscience and Remote Sensing*, 37(1), 135–149.

Tukey, J.W. (1977) *Exploratory Data Analysis*. Addison-Wesley Publishing Company, Reading MA, USA, 688 pp.

Umarhadi, D.A., Avtar, R., Widyatmanti, W., Johnson, B.A., Yunus, A.P., Khedher, K.M., Singh, G. (2021) Use of multifrequency (C-band and L-band) SAR data to monitor peat subsidence based on time-series SBAS InSAR technique. *Land Degradation & Development*, 32(16), 4779–4794.

Van Asselen, S., Erkens, G., de Graaf, F. (2020) Monitoring shallow subsidence in cultivated peatlands. *Proceedings of the International Association of Hydrological Sciences*, 382, 189–194.

Webley, P.W., Wadge, G., James, I.N. (2004) Determining radio wave delay by non-hydrostatic atmospheric modelling of water vapour over mountains. *Physics and Chemistry of the Earth, Parts A/B/C*, 29(2–3), 139–148.

Webster, K.L., Bhatti, J.S., Thompson, D.K., Nelson, S.A., Shaw, C.H., Bona, K.A., Hayne, S.L., Kurz, W.A. (2018) Spatially-integrated estimates of net ecosystem exchange and methane fluxes from Canadian peatlands. *Carbon Balance and Management*, 13(1), 16, 21 pp.

Wei, M., Sandwell, D.T. (2010) Decorrelation of L-band and C-band interferometry over vegetated areas in California. *IEEE Transactions on Geoscience and Remote Sensing*, 48(7), 2942–2952.

Weydahl, D.J. (2001) Analysis of ERS tandem SAR coherence from glaciers, valleys, and fjord ice on Svalbard. *IEEE Transactions on Geoscience and Remote Sensing*, 39(9), 2029–2039.

Yu, Z.C. (2012) Northern peatland carbon stocks and dynamics: a review. *Biogeosciences*, 9(10), 4071–4085.

Zhou, Z. (2013) Chapter 4: Mapping the eroding extent and severity of peatland surface over the Monadhliath Mountains, Scotland. In: *The Applications of InSAR Time Series Analysis for Monitoring Long-term Surface Change in Peatlands*. PhD thesis, University of Glasgow, UK, 231 pp.

Zhou, Z., Waldron, S., Li, Z. (2010) Integration of PS-InSAR and GPS for monitoring seasonal and long-term peatland surface fluctuations. In: *Remote Sensing and the Carbon Cycle*, Proceedings of the Remote Sensing and Photogrammetry Society Conference, Burlington House, London, UK (Volume 1), 4 pp.

Submitted 09 Jun 2022, final revision 06 Aug 2023
Editor: Olivia Bragg

Author for correspondence:
Dr Tauri Tampuu, Department of Geography, Institute of Ecology and Earth Sciences, University of Tartu and KappaZeta Ltd., Tartu, Estonia. Email: ttampuu@ut.ee

Appendix

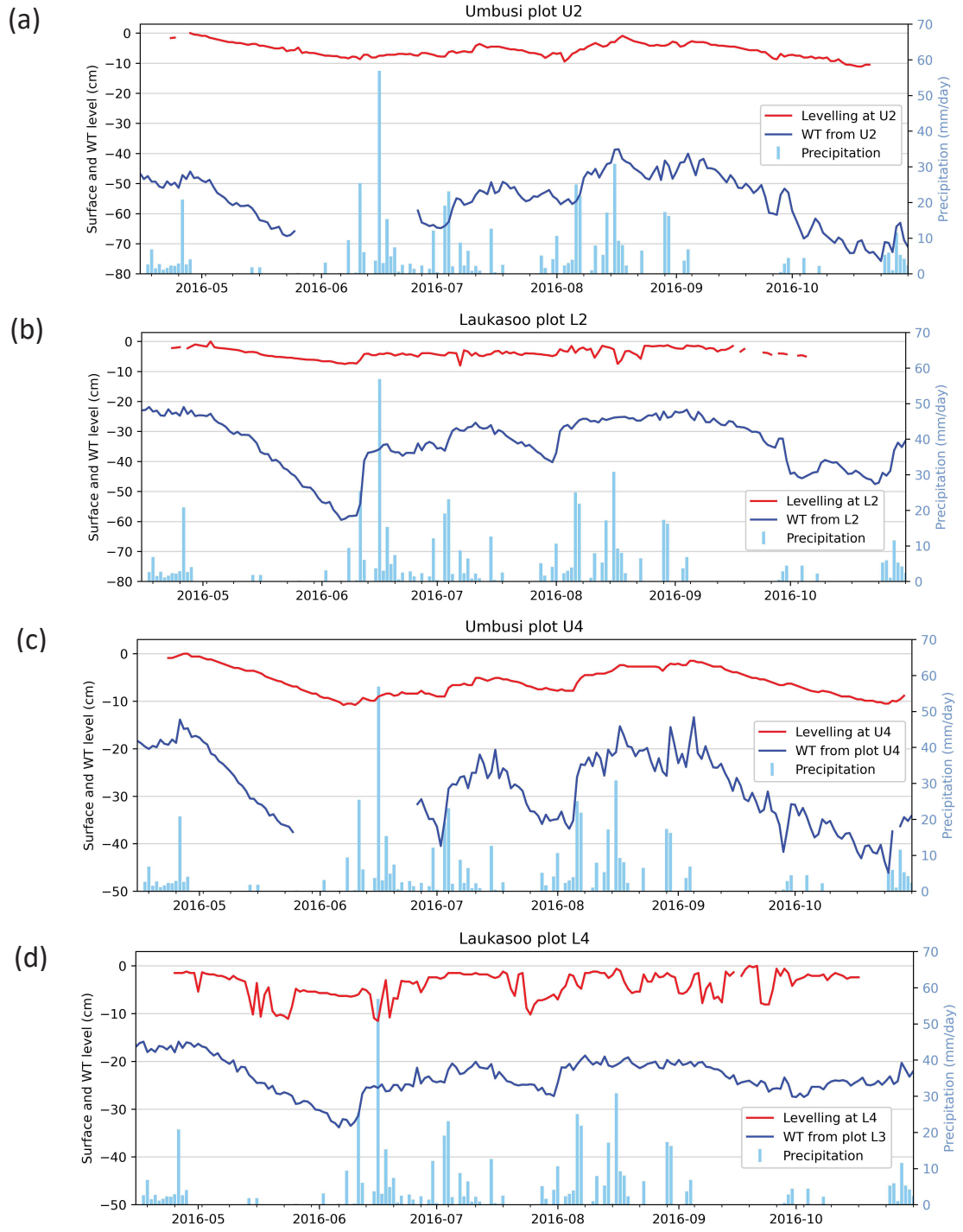

Figure A1. Daily medians of peatland surface height and daily averages of peatland water table (WT) for plots in Umbusi Bog and Laukasoo Bog where levelling data are available, along with daily precipitation totals, during the growing season 15 Apr–31 Oct 2016. Plots U2 (a) and L2 (b) are haplotelmic; U4 (c) and L4 (d) are a lawn nanotope in Umbusi and and a hollow nanotope in Laukasoo, respectively, that are significantly affected by drainage. The levelling data are shown relative to the maximum surface height of the period, and the WT data relative to the peatland surface at the time of measurement. The WT record from Plot L3 in Laukasoo Bog is used to represent the WT at L4.

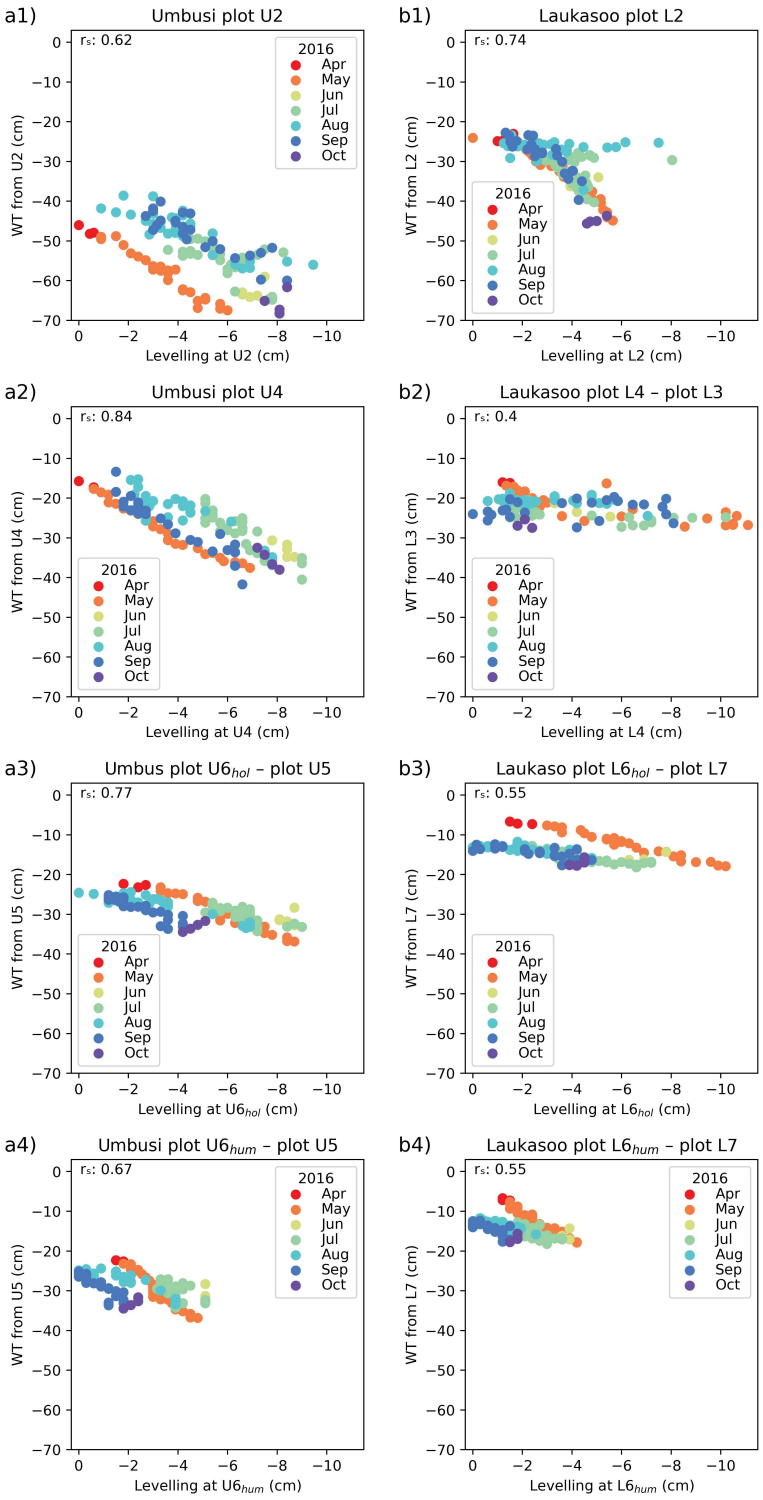

Figure A2. Correlations (r_s; p-value < 0.001) between the daily median peatland surface height and daily average of peatland water table (WT) during the growing season 15 Apr–31 Oct 2016. The number of days correlated is 123. The levelling data are shown relative to the maximum surface height of the period and WT is relative to the peatland surface at the time of the measurement. The letters "U" and "L" (together with the plot identifier) denote measurement plots along the drainage gradient in Umbusi Bog and Laukasoo Bog, and levelling measurements from hollow and hummock nanotopes are denoted by the subscripts "hol" and "hum", respectively. WT data from Plots U5, L3 and L7 are used to represent the WT at U6, L4 and L7, respectively.

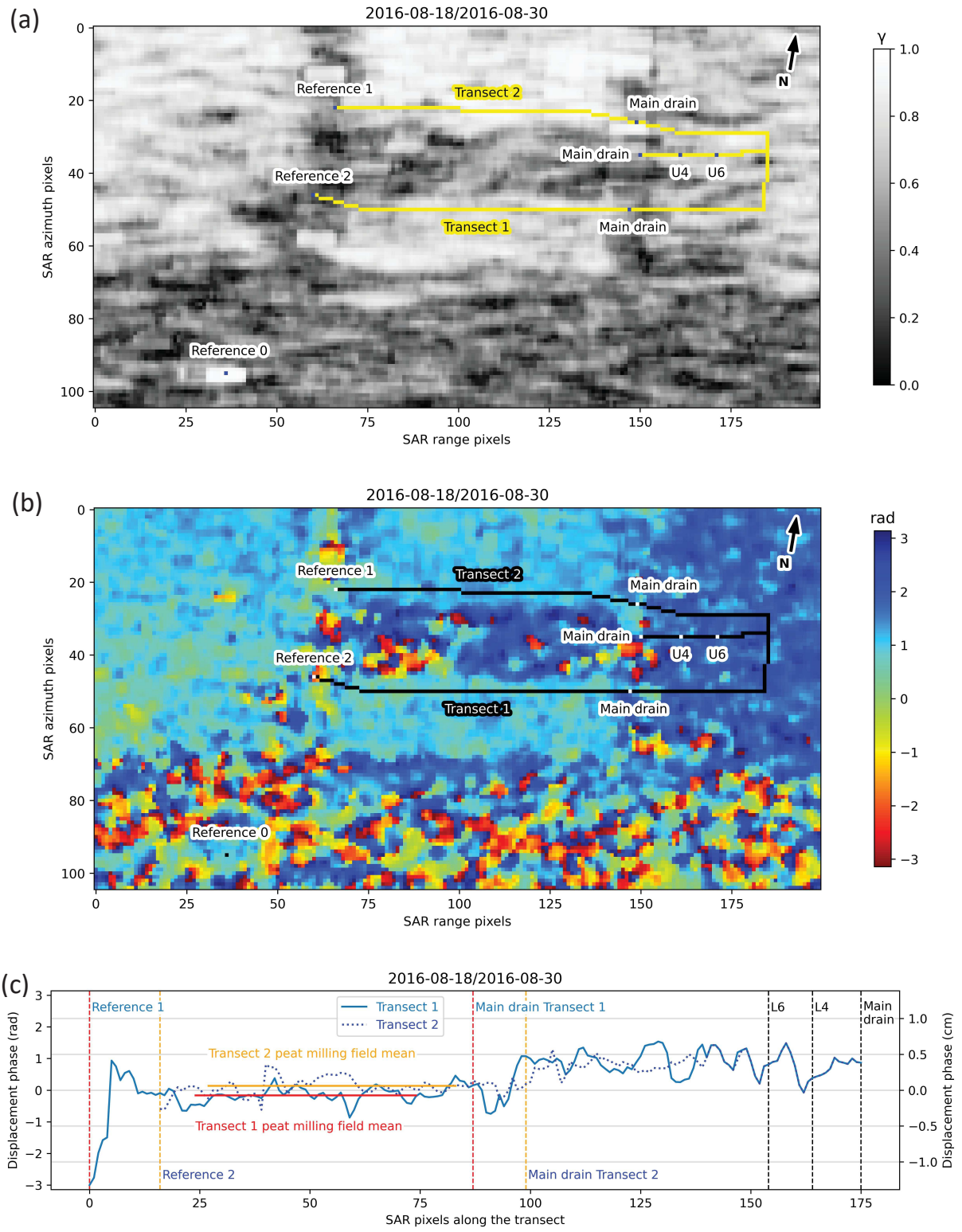

Figure A3. Laukasoo Bog: InSAR coherence γ (a) and phase (b) images and radar line of sight deformation along the virtual transects (c) in radar coordinates for the image pair 18–30 Aug 2016. Stable reference points used in DInSAR processing and the plots (L4 and L6; ground levelling data available) used in validation of DInSAR deformation estimates are indicated. The geographic coordinates of the scene are shown in Figure 1.

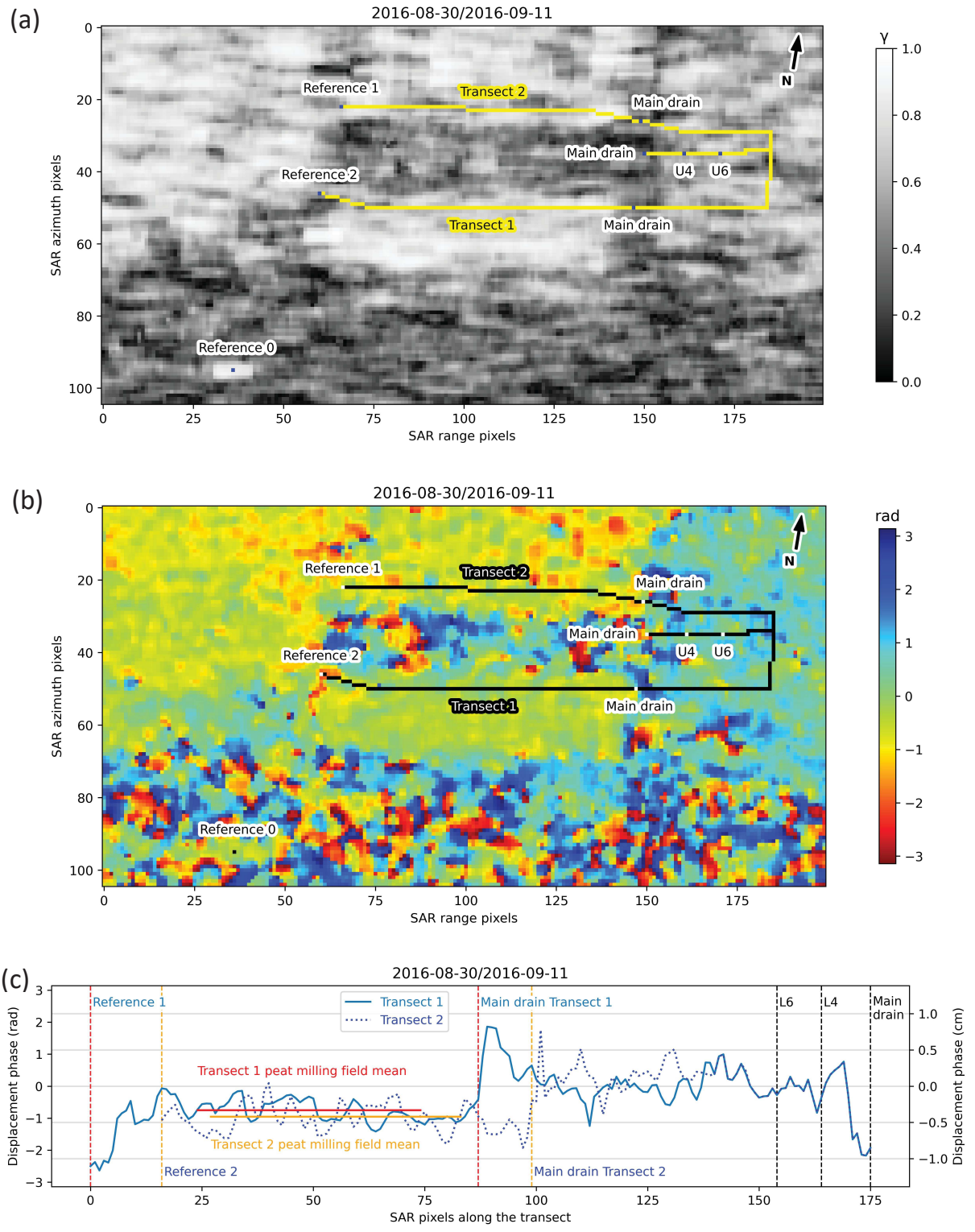

Figure A4. Laukasoo Bog: InSAR coherence γ (a) and phase (b) images and radar line of sight deformation along the virtual transects (c) in radar coordinates for the image pair 30 Aug–11 Sept 2016. Stable reference points used in DInSAR processing and the plots (L4 and L6; ground levelling data available) used in validation of DInSAR deformation estimates are indicated. The geographic coordinates of the scene are shown in Figure 1.